SYNTHESIS AND CHARACTERIZATION OF Ni-Cu/RGO NANOCOMPOSITE FOR METHANOL ELECTRO -OXIDATION

MSc THESIS

YITBAREK SHIGUTIE BALCHA

NOVEMBER 2017

HARAMAYA UNIVERSITY, HARAMAYA

Synthesis and Characterization of Ni-Cu/RGO Nanocomposite for Methanol Electro-Oxidation

A Thesis Submitted to the Department of Chemistry, Postgraduate Program Directorate

HARAMAYA UNIVERSITY

In Partial Fulfillment of the Requirements for the Degree of

MASTER OF SCIENCE IN CHEMISTRY

Yitbarek Shigutie Balcha

November 2017

Haramaya University, Haramaya

HARAMAYA UNIVERSITY

POSTGRADUATE PROGRAM DIRECTORATE

I hereby certify that I have read and evaluated this Thesis prepared under my guidance, by **YITBAREK SHIGUTIE BALCHA**, entitled: **SYNTHESIS AND CHARACTERIZATIO-N OF Ni-Cu /RGO NANOCOMPOSITE FOR METHANOL ELECTRO-OXIDATION.** I recommend that it be submitted as fulfilling the Thesis requirement

Abebaw Adgo (PhD)	_____	_____
Major Advisor	Signature	Date
Abi Taddesse (PhD)	_____	_____
Co-Advisor	Signature	Date

As a member of the board of examiners of the MSc Thesis Open Defense Examination, I certify that I have read, evaluated the thesis prepared by **Yitbarek Shigutie Balcha** and examined the candidate. I recommend that the thesis is accepted as fulfilling the thesis requirement for the degree of **Master of Science in Chemistry.**

_____	_____	_____
Chairperson	Signature	Date
_____	_____	_____
Internal Examiner	Signature	Date
_____	_____	_____
External Examiner	Signature	Date

DEDICATION

I dedicate this Graduate thesis manuscript to my mother W/ro Zenebech Debele, for nursing me with affection and love and for her dedicated partnership in the success of my life.

STATEMENT OF THE AUTHOR

By my signature below, I declare and affirm that this Thesis is my own work. I have followed all ethical and technical principles of scholarship in the preparation, data collection, data analysis and compilation of this Thesis. Any scholarly matter that is included in the Thesis has been given recognition through citation.

This thesis is submitted in partial fulfilment of the requirements for an MSc degree. It is made available to borrowers under the rules of Haramaya University Library. I solemnly declare that this Thesis has not been submitted to any other institution anywhere for the award of any academic degree, diploma or certificate.

Brief quotation from this Thesis may be made without special permission provided that accurate and complete acknowledgement of source is made. Requests for permission for extended quotation from or reproduction of this Thesis in whole or part may be granted by the Head Department or Director of the Postgraduate Program Directorate when in his or her judgment the proposed use of material is in the interest of scholarship. In all other instances, however, permission must be obtained from the author of the Thesis.

Name: Yitbarek Shigutie Signature_____

Date: November 2017

Department: Chemistry

BIOGRAPHICAL SKETCH OF THE AUTHOR

The author was born from his father Shigutie Balcha and his mother Zenebech Debele Bedhane on August 29, 1986 in Oromia Regional State, Arsi Zone, Tena Woreda. He started his primary education in Korobta Lemlem Elementary School in 1993. He attended his secondary school in Didea Robe Secondary and Preparatory School. After completing preparatory school, he then joined Addis Ababa University, Department of Chemistry in 2004 and graduated with BSc degree in Chemistry in 2006. Soon after graduation, the author was employed by MoE in 2007 to work under Oromia Education Bureau, in Arsi zone, in Arsi Robe Woreda as a teacher. After five years of service, he joined Haramaya University, College of Natural and Computational Sciences, Department of Chemistry in 2012 to pursue his postgraduate studies in Chemistry.

ACKNOWLEDGEMENTS

Above all, I would like to praise the Almighty God for bestowing up on me health, strength, patience and protection throughout the study period.

Next, I would like to express my deepest gratitude to my major advisor Dr. Abebaw Adgo for his limitless help and timely advices, valuable and constructive comments, close supervision throughout the study.I would to like express also my deep sense of gratitude to my co- advisor Dr.Abi Taddesse for his patience in following up this work from the very beginning up to the end.

My special heartfelt thanks also goes to Dr. Endale Teju for his fatherly approach, guidance, coordination, valuable comments, suggestions, encouragement and in correcting my paper especially during proposal stage.

My special thanks also goes to Dr.Efrem Taddesse & Dr.Neelaiah Babu.G for their guidance and encouragement.

I would like to extend my gratitude to Dr.Yonas Chebude and Dr.Negash, Addis Ababa University, Department Of Chemistry a for running the samples

My sincere gratitude goes to Mr.Zewdu Bezu, W/ro Yanchiamilak Adamu, Ato Kase Desalegn, W/roWeynshet Alamaw and other staffs of Chemistry Department of Haramaya University, for their friendly approach, guidance and giving me access to the laboratory and instrumentation facilities. The author also wishes to thank the Directors of Didea Robe Preparatory school, namely Ato Debebe Negash and Ato Taye Tamiru, for their paying special respect to me and providing me permission during my laboratory research work

Finally, my heartfelt appreciation extends to all members of my family, Ato Lema Debele and Ato Digafe Legese for their financial support.

ACRONYMS AND ABBREVIATIONS

AFC	Alkaline Fuel Cells
AEMFC	Anion Exchange Membrane Fuel Cell
CA	Chronoamperometry
Cu-RGO	Copper- Reduced Graphene Oxide nanocomposite
CE	Counter Electrode
CV	Cyclic voltammetric
DMFC	Direct Methanol Fuel Cell
EIS	Electrochemical Impedance Spectroscopy
EDX	Energy Dispersive X-ray analysis
FTIR	Fourier Transform Infra Red
MFC	Methanol Fuel Cell
MOR	Methanol Oxidation Reaction
MCFC	Molten Carbonate Fuel Cell
Ni-Cu	Nickel-Copper nanoparticle
Ni-Cu/RGO	Nickel-Copper Reduced Graphene Oxide nanocomposite
Ni-RGO	Nickel- Reduced Graphene Oxide nanocomposite
PAFC	Phosphoric Acid Fuel Cell
PEG	PolyEthylene Glycol
PEMFC	Polymer Electrolyte Membrane Fuel Cell
RE	Reference Electrode
SEM	Scanning Electron Microscopy
SOFC	Solid Oxide Fuel Cell
Uv-Vis	Ultraviolet-visible
WE	Working Electrode
XRD	X-Ray Diffraction

TABLE OF CONTENTS

LIST OF TABLES

LIST OF FIGURES

Figure **Page**

LIST OF TABLES IN THE APPENDIX

Tables **Page**

LIST OF FIGURES IN THE APPENDIX

Synthesis and Characterization of Ni-Cu/Reduced Graphene Oxide Nanocomposite for Methanol Electro-oxidation

ABSTRACT

Ni-Cu/reduced graphene oxide (RGO) nanocomposite was prepared by using chemical reduction method for methanol electro-oxidation. Ni-RGO and Cu-RGO were also synthesized using the same method to compare their performance for methanol electro-oxidation. The synthesized nanocomposites Ni-RGO, Cu-RGO and Ni-Cu/RGO were characterized using x-ray diffraction (XRD), scanning electron microscopy (SEM), Fourier transform infrared spectroscopy (FTIR), Energy dispersive X-ray spectroscopy (EDX) and ultraviolet-visible spectroscopy (Uv-vis). Electrochemical properties of the nanocomposites were studied by employing cyclic voltammetry (CV), chronoamperometry and electrochemical impedance spectroscopy (EIS). Ni-Cu/RGO exhibited a superior electrocatalyst towards methanol oxidation in alkaline medium as evidenced from its high current density (440 mA) compared to that of Ni-RGO (353 mA) and Cu-RGO (242 mA). This is probably because of Ni-Cu/RGO nanocomposites high electrocatalytic surface area (89.1cm^2/g) and the synergetic catalytic effect coming from both Ni and RGO. Besides, Ni-Cu/ RGO may be tolerance to the poisoning effect from intermediates accumulated on the surface of the electrode during the redox reaction. The effect of scan rate on methanol oxidation on surface of Ni-Cu/RGO was also investigated using CV. It was noticed that the peak current increased with scan rate while peak potential slightly shifted toward a more positive value. Moreover, plot of peak current versus square root provided a straight line indicating the reversibility of the process. The diffusion coefficient of methanol was found to be 2.6x$10^{-4}$$cm^2$/s. Furthermore, the Ni-Cu/ RGO study using EIS demonstrated fast electron transfer kinetics in comparison to those of the binary systems. Therefore, Ni-Cu/RGO nanocomposite is a new electrode material and it can be utilized for the electrochemical oxidation of methanol in fuel cells.

Keywords: Bimetallic nanocatalysts, Reduced graphene oxide, Methanol oxidation

1. INTRODUCTION

A rapidly growing population and industrialization has caused the world's natural resources difficulty in keeping up with demands. Today, fossil fuels such as coal, oil or natural gas (i.e., hydrocarbons) are burned in power plants to produce energy. Primarily 27 % of world energy comes from coal (Minh, 2011). The use of coal, oil or any hydrocarbon fuel leads to the generation and release of carbon, nitrogen and sulfur oxide gases into the atmosphere causing air pollution and ozone layer depletion (Geng, 2012). It has been observed that the ozone in the earth's atmosphere is deteriorating and create a big hole that allow the transmission of more harmful ultraviolet rays to the environment (Asanda, 2010). Chlorofluorocarbons (CFC) and nitrogenous oxides are responsible for the deterioration of ozone. On the other hand, emission of CO_2 gas into the atmosphere has been linked to global warming So, to avoid generation of carbon monoxides, carbon dioxide and other harmful pollutants, there is a direct need to look at alternate sources of energy that favor cleaner fuels, including fuel cells, solar technologies (photovoltaic), wind turbines, tidal systems etc. Fuel cells are one of the emerging technology that can meet these demands (Asanda, 2010).

A fuel cell is defined as an electrochemical energy conversion device that produces electricity from chemical reaction. It was possible to continuously provide the fuel and oxidant into the fuel cell and was a characteristic that makes it different from other devices such as Batteries. In fuel cells Conversion of chemical energy is directly converted to electrical energy while in combustion engines chemical energy was first converted to mechanical energy then to electrical energy (Antolini *et al.,* 2006).

There are several types of fuel cells, which are classified according to the type of electrolyte they use which governs the operating temperature and the catalyst suitable for those conditions must then be selected. Among the various types of fuel cells, Methanol Fuel Cell (MFC) is the most attractive, using liquid and renewable methanol as a fuel. MFCs have been considered to be a very promising alternative in terms of fuel usage and feed strategies. Unlike hydrogen-fed fuel cells, which have safety, storage, and distribution challenges and Ethanol fuel cell, the platinum-based catalyst is very expensive, MFC uses liquid methanol as a fuel and can easily be stored, reformed

and transported. This therefore simplifies the fuel cell system (Andisiwe, 2013). It has received much attention over the years as a promising technological development that can replace conventional batteries as power sources for portable devices. This is due to their unique features of using liquid methanol as a fuel which offers, high specific energy density, high energy conversion efficiency of 40-50 %, low operating temperatures (0 -100 ℃) and the use of methanol as a fuel allows for easy storage and transportation , something which simplifies the fuel cell system (Ezhil *et al.*, 2016). Their full commercialization, however, is still hindered by the: 1) use of perfluorosulfonic acid membranes, such as Nafion, which allow methanol, together with water, to permeate through the membrane from the anode to the cathode. This phenomenon is referred to as 'methanol cross-over', the methanol that crosses over reacts with oxygen at the cathode and reduces the cathode potential, with the end results being that less power is generated by the fuel cell and can lead to a waste of fuel; and 2) the sluggish electro-kinetics of the methanol oxidation (MOR) at the anode which is mainly caused by the poisoning of the Pt catalyst by carbon monoxide (CO), a by-product of methanol oxidation which blocks the active site of the platinum catalyst, resulting in slow kinetics (Zhao *et al*., 2010). MFCs also available at very high cost because of the electrocatalyst used which is platinum based and can be very expensive. This can be overcome by using reduced amounts of the catalyst without reducing the efficiency of the cell or using non platinum based catalysts (Trasatti *et al.*, 1981).

A large number of electrocatalysts have been used for oxidation of methanol, which among them the electrocatalysts based on Pt nanocomposite such as CuPt, PtRu, PtNi, PtSn, PtMo, Pt-Au/RGO, ternary alloy, PtRuNi, and PtRuMo (Abdel *et al.*,2004; Gyenge, 2008;Kamarudin *et al.*, 2009; Vishal *et al*., 2011; Rahul *et al*., 2016) have a good activity for methanol oxidation, but adsorption of carbon monoxide on Pt tends to slow down the kinetics of oxidation reaction and in addition, the high cost of Pt metal was another limitation (Ferdowsi *et al.*,2015). Therefore, many attempts have been made toward the examination of the catalytic activity of cheap metals such as copper-based materials. Thus, bimetallic Cu-based alloys with Cu rich composition experimentally have been extensively used to improve CO_2 electro-reduction owing to high overpotential and low current density of the pure Cu surface, such as Cu–Ni, Cu–Zn, Cu–Cd, Cu–Sn, Cu–Pb, Cu–Au, Cu–Ag, Cu–Pd, Cu–Pt (Jafarian *et al*., 2006;

Schumacher *et al.*, 2008; Subramanian *et al.*, 2009; Xu *et at*., 2012; Duhong *et al*., 2015; Zhao *et al*., 2015). Within this context, nickel has been suggested for substituting the platinum in anodes and cathodes of MFCs because of the similarities between these metals, as well as the major abundance and low cost of Ni (Jurzinsky *et al.*, 2016). Moreover, despite the excellent results obtained with the $Ni/Ni(OH)_2/$ there are two main limitations regarding their application in electro oxidative processes of methanol. The first one was due to the significant deactivation of the $Ni/Ni(OH)_2/$ electrode surface, when large methanol concentrations were used. The second was the formation of γ-NiOOH species during long cycling electro oxidative processes, which were ineffective to catalyze the alcohol oxidation.

Taking into account these limitations, it becomes necessary to move towards an optimal utilization of the electro active catalyst on the electrode in terms of selectivity and reaction conversion. According to the literature, different strategies are being investigated to improve the catalytic activity of NiOOH species, including the use of alloys of metallic Ni with other metals such as Ti, Cu and Ru, or the dispersion of the metallic species on different carbonaceous supports (Leticia *et al*., 2014). Among various alloys, Ni–Cu nanoalloys are particularly efficient electrocatalysts for a number of reactions including methane decomposition, methanol oxidation, and $NaBH_4$ hydrolysis to generate hydrogen (Ruimin *et al.*, 2011).

The performance of a MFC is essentially governed by the electrocatalyst support materials as they strongly influence the electrocatalyst performance, durability and efficiency (Chia-Liang *et al*., 2014). A variety of carbon based materials (carbon black, carbon nanotubes, mesoporous carbon, or graphene) have attracted great attention as the electrocatalyst support in methanol oxidation for fuel cell application. This can strengthen the dispersion and stability of the metal nanoparticles, which enhances the catalytic stability, activity and selectivity. Among various supports, carbon materials have attracted great attention as catalyst supports in fuel cells due to their unique electrical, thermal, and micro/mesoporous properties (Vishal *et al*., 2011). The activity and durability of carbon-supported nanoparticle in methanol oxidation reactions were of great concern. Recently, graphene (reduced graphene oxide, RGO) has

attracted attention as a unique 2D material with low cost, high surface area, good electrical conductivity and high mechanical strength, which could not only maximize the availability of a nano sized electro catalyst surface area for electron transfer, but could also provide enhanced mass transport of reactants to the electro catalyst (Tang *et al.,* 2009). To the best of our knowledge, there is no report available on Ni-Cu/RGO nanocomposite for methanol electro-oxidation. Therefore, in this study, the synthesis of Ni-Cu/RGO nanocomposite and the electrocatalytic activity towards methanol oxidation is reported. The catalytic activity of the as prepared Ni-Cu/RGO nanocomposite for methanol oxidation has been studied using cyclic voltammetry (CV), linear sweep voltammetry (LCV), chronoamperometry (CA) and electrochemical impedance spectroscopy (EIS) measurements techniques.

Objectives of the Study

General Objective

To develop an efficient bimetallic Ni-Cu/reduced graphene oxide nanocomposite and apply as electrocatalyst for methanol oxidation.

Specific Objectives

- To synthesize Cu/reduced graphene oxide, (Cu-RGO) nanocomposite
- To synthesize Ni/reduced graphene oxide, (Ni-RGO) nanocomposite
- To synthesize Ni-Cu/reduced graphene oxide, (Ni-Cu/RGO) nanocomposite at room temperature.
- To characterize as synthesized Cu-RGO, Ni-RGO and Ni-Cu/RGO nanocomposites using, Uv-vis, FTIR, XRD and SEM.
- To study the electrocatalytic activity of the Cu-RGO, Ni-RGO and Ni-Cu/RGO for methanol oxidation using CV, LSV, CA and EIS.

2. LITERATURE REVIEW

2.1. Fuel Cells

The first fuel cell was discovered by Sir William Grove in 1839, and he is widely acknowledged as the "Father of Fuel cells". Grove was interested in reversing the process of electrolysis which is precisely what happens in fuel cells (Alexandre, 2005). A fuel cell is an electro-chemical device that directly converts the free energy of a chemical reaction of a fuel (e.g. hydrogen, natural gas, methanol, gasoline, and formic acid) and an oxidant (air or pure oxygen) into electrical energy.

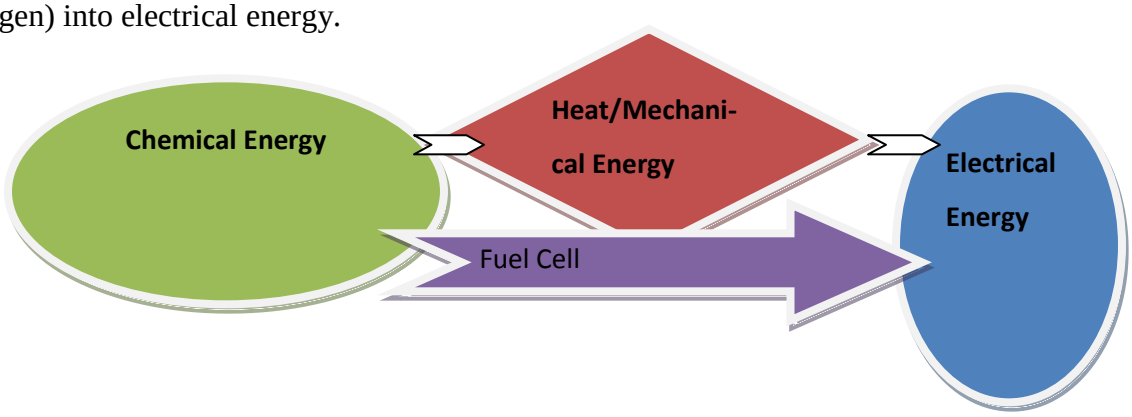

Figure 1. The different energy conversion paths

Oxidation of the fuel takes place on the anode and reduction occurs on the cathode of the fuel cell (Paganin *et al.*, 2005). The increased demand for energy has led to an increase in the cost of fuels. In response to the pressing global concerns relating to sustainable generation of energy and increasing population therefore, a strong research drive has been mounted globally to develop environmentally clean and efficient alternatives to fossil fuel, and fuel cells were proving to be an interesting and very promising alternative, which can realize the promise of clean reliable electric power generation with high efficiency. The type of electrolyte material employed governs their performance characteristic, making each type of fuel cell suitable for specific applications. Fuel cells were generally characterized by the type of electrolyte, the operation temperature, the type of ion transport, or the fuel-type. A summary of fuel cell types is presented in Table 1(Jordan, 2012).

Table1.Summary of the Major Fuel Cell Types

	PEMFC	AFC	AEMFC	DMFC	PAFC	SOFC	MCFC
Electrolyte	Polymer membrane	Aqueous membrane	Polymer membrane	Polymer membrane	H_3PO_4 Alkali solution	Ceramic oxide	Molten carbonate
Operation Temp.^{0}C	50-100	50-200	50-100	20-90	150-220	700-1000	600-700
Charge Carrier	H^+	OH^-	OH^-	H^+	H^+	O^{2-}	CO^{2-}
Catalyst	Pt	Pt	Pt	Pt-Pt/Ru	Pt	Ni	Ni
Primary Fuel	H_2	CH_3OH	H_2	H_2	H_2	H_2 CO CH_4	H_2 CH_4
Combined Cycle (%)	50-60	50-60	50-60	30-40	55	55-65	50-60
Primary Application	Automotive/ Stationary	Military, Space	Automotive /Stationary	Portable Power, Transportation	Stationary	Automotive /Stationary	Stationary

2.1.1. Methanol for Fuel Cells

Methanol fuel cell is one of the most promising devices for energy sources. It offers several advantages over other types of fuel cells in that it is a dependable and long lasting portable power source that can replace batteries in a number of electronic products, including laptop computers and cellular phones (Andisiwe, 2013). Some of the unique features that make MFC to be viewed by many as a key enabling technology for this century include (Qiu *et al.*, 2011): High energy density of liquid methanol (6100 $Whkg^{-1}$ at 25 ℃); High energy conversion efficiency (40-50 %); Ease of delivery and storage of liquid methanol; Low temperature of operation (0-100 ℃)$^{;}$ Simple and compact structures; and availability of liquid methanol Liquid methanol can be sourced from fossil fuels, such as natural gas or coal, as well as from

sustainable sources through fermentation of agricultural products and biomasses (Lu and Wang, 2004). Methanol is easily available. The low cost of liquid methanol and the fact that it can be distributed using the present infrastructure for liquid fuels eliminates the need to build new infrastructure and accordingly, it reduces the high cost that goes with building new infrastructure.

2.1.2. Working Principle of the Methanol Fuel Cell

Electrochemical reactions occur in the catalyst layers (CLs), which are attached to both sides of the membrane. They are designed in such a manner as to facilitate the transport of protons, electrons and reactants. The function of the membrane is to conduct protons from the anode to the cathode and simultaneously serve as an insulator for electrons. The methanol solution is supplied as a fuel to the anode flow channel and transfers from the anode diffusion layer (DL) to the anode catalyst layer (CL) where it is electro-chemically oxidized in the presence of a catalyst typically binary nanocomposite to form protons, electrons and carbon dioxide and the remaining methanol solution was transported to the cathode catalyst layer through the polymer electrolyte membrane.

The permeation of methanol from anode to cathode was referred to as methanol cross-over, which creates mixed potential and decreases the cathode potential (Arico *et al*., 2001). The produced carbon dioxide in the anode catalyst layer (CL) then moves backward through the anode diffusion layer to the flow channel as shown in Fig.2 below and from there it was vented out by a stream of liquid solution toward the exit of the flow channel. The protons, formed at the anode catalyst layer, are transported through the polymer electrolyte membrane to the cathode catalyst layer (CL). Since the membrane serves as an insulator for electrons, therefore, electrons commence their journey across the external circuit arriving at the cathode, depleted from having performed external work. On the cathode, oxygen/air is supplied through the cathode flow channel and was transferred from the cathode diffusion layer (DL) to the cathode catalyst layer (CL).

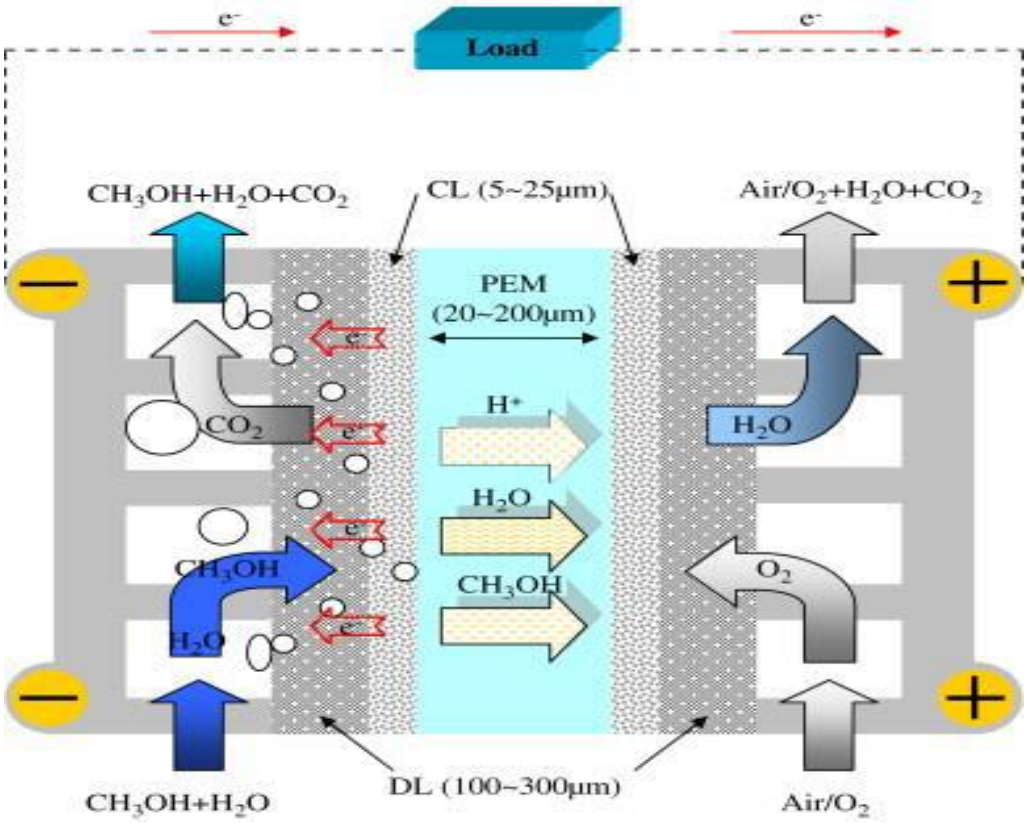

Figure 2. Schematic representation of a methanol fuel cell

This was where the majority of oxygen reacts with electrons and protons in the presence of a catalyst, typically pure Cu on highly conductive carbon support to form water while the remaining part of oxygen electro-chemically reacts with the permeated methanol (Asanda, 2010).

The overall half-cell reaction at the anode was

$$CH_3OH + H_2O \longrightarrow CO_2 + 6H^+ + 6e^- \quad E^\circ = 0.046V$$

At the cathode the overall half-cell reaction was

$$6H^+ + 6e^- + 3/2O_2 \longrightarrow 3H_2O \qquad E^\circ = 1.23V$$

Thus, the overall cell reaction in the MFC is

$$CH_3OH + 3/2O_2 \longrightarrow CO_2 + 2H_2O \quad E^\circ = 1.184V$$

Means, that methanol reacts with oxygen to produce the desired electrical energy with carbon dioxide and liquid water as by-products. The standard cell voltage for a MFC at 25 ^{o}C is 1.184 V. However, this potential is never achieved practically. Instead, the open circuit potential is usually about 0.6 to 0.8V in the best case (Asanda, 2010).

2.2. Electrocatalyst for Methanol Oxidation

An electrocatalyst is a catalyst that participates in electrochemical reactions and was used to modify the rate of chemical reactions without being consumed in the process. After the reaction, it can theoretically be recovered from the reaction mixture chemically unchanged. They assist in transporting electrons between the electrode and reactants and/or facilitate an intermediate chemical transformation described by an overall half-reaction. An electrocatalyst can be heterogeneous, such as platinum surface or nanoparticles or homogeneous, like enzyme. For low temperature fuel cells, nickel was considered to be the catalyst of choice for both anode and cathode fuel cell reactions. In pursuit of improving the oxidation reduction reaction catalyst activity, nickel was usually alloyed with a first row transition and second row transition metal forming binary electrocatalyst (Ni- Fe, Cu -Ni, Ag -Ni, etc.) or use ternary electro-catalysts (Pt-Ni-Fe, Ni -Cu -P, etc.) (Andisiwe, 2013).

2.2.1. Reaction Mechanism of Methanol Electro-oxidation

The MOR, catalysed by Ni-Cu catalyst, was assumed to follow through two mechanisms, namely: the bifunctional effect and the ligand effect. The bifunctional effect involves de-hydrogenation of the adsorbed methanol molecule to form poisonous intermediate CO, which further becomes adsorbed on the Cu surface. The Ni atoms provide sites for water adsorption and dissociation, thus, forming oxygen-containing species on Ni sites and this promotes the oxidative removal of CO_{ads} to CO_2 in that involves the following steps:(1) methanol adsorption (2) C-H bond activation (methanol dissociation) (3) water adsorption (4) water activation (5) CO oxidation. The formation of Ni-OH by water was a key step for the oxidative removal of adsorbed CO (Geng, 2012).

$$Cu + CH_3OH \longrightarrow Cu\text{-}(CH_3OH)_{ads}$$

$$Cu\text{-}(CH_3OH)_{ads} \longrightarrow Cu\text{-}(CH_3O)_{ads} + H^+ + e^-$$

$$Cu\text{-}(CH_3O)_{ads} \longrightarrow Cu\text{-}(CH_2O)_{ads} + H^+ + e^-$$

$$Cu\text{-}(CH_2O)_{ads} \longrightarrow Cu\text{-}(CHO)_{ads} + H^+ + e^-$$

$$Cu\text{-}(CHO)_{ads} \longrightarrow Cu\text{-}(CO)_{ads} + H^+ + e^-$$

Then incorporate the second metal element can provide oxygenated species at lower potentials, binary Cu based alloys have been investigated towards methanol oxidation. Ni-Cu seems to be the most active and the state-of-the art anode catalyst for MFCs.

$$Ni + H_2O \longrightarrow Ni\text{-}(H_2O)_{ads}$$

$$Ni\text{-}(H_2O)_{ads} \longrightarrow Ni\text{-}(OH)_{ads} + H^+ + e^-$$

$$Ni\text{-}(OH)_{ads} + Cu\text{-}(CO)_{ads} \longrightarrow Ni\text{-}Cu + CO_2 + H^+ + e^-$$

2.2.2. Nanoparticles for Methanol Electrocatalysis

The nanoparticle requirements for a fuel cell are that, it must have high activity for the electro-oxidation of fuel at the anode and for the electro-reduction of oxygen molecule at the cathode electrode of the cell. Stability and good electric conductivity to minimize resistive losses on the nanoparticle layer is also required. The nanoparticle should also be less expensive in order to minimize the overall costs of the fuel cell. Presently low cost, nickel and nickel based electrocatalysts are considered as the most active electrocatalyst for both electro-reduction of oxygen at the cathode and electro-oxidation of methanol at the anode. The choice of copper-nickel nanoparticle as electrocatalyst was due to the fact that they possess good catalytic, electronic and magnetic properties. Also, they were widely used for industry applications, due to their excellent resistance to corrosion, high inherent resistance to biofueling and good fabrication (Arul *et al*., 2014).

2.2.3. Binary Metallic Nanomaterial

Electroactivity in methanol fuel cell anode electrode was one of the major challenges for this type of fuel cells because of the slow kinetics of methanol oxidation. The half cell reaction on this electrode

$$\mathbf{CH_3OH + H_2O \rightarrow CO_2 + 6H^+ + 6e^-}$$

Indeed very few electrode materials have been shown capable of adsorbing methanol in basic media and, of these Platinum based materials display enough stability and activity were attractive as fuel cell electrocatalyst. The main challenge with using platinum metal as a catalyst was the sensitivity of the metal catalyst to carbon monoxide poisoning. CO, an intermediate of methanol oxidation which was adsorbed strongly on the surface of Pt and blocks the catalytically active area of Pt and in so doing significantly decreases its reactivity, resulting in sluggish electro-kinetics and low catalytic efficiency. Various Ni based alloys such as Ru-Ni, Au-Ni, Ag-Ni, Pd-Ni, and Ni-Cu have been investigated in order to improve the efficiency of methanol (Andisiwe, 2013). Among them, Ni-Cu alloy with the atomic ratio of 0.7:0.3 acts as an effective catalyst for the oxidation of methanol in an alkaline process, and has been found to have better performance because of its suitable structural composition, alloying degree, particle size and morphology (Ruimin *et al.*,2011).

Table 2 . The various bimetallic electrocatalyst for methanol oxidation

Nanopar-ticle	Size (nm)	Support/loading	Preparation method	Advantage	Disadvantage	References
Pt-Ru	2.5-5	carbonnanofibers	reduction by NaBH4	increase the activity Per unit area	-Cost of Pt precursor	Maiyalagan, 2009
Pt/MnO_2	2.9	RGO	reduction by NaBH4	superior electrochemical active surface area	Cost of Pt precursor	Qizhong *et al*., 2015
Ni–MgO	16.8	-	electrodeposition	low cost	Poisoning effect a lower charge transfer resistance	Hassan *et al*.,2016
Co-Cu	25	carbon nanofibers	electro spinning of a sol–gel	non-precious catalysts	The electro spinning process can be efficiently utilized to produce carbon nanofibers decorated by metallic nanoparticles	Nasser *et al* ., 2014
Cu_2O/Pd	10	-	chemical precipitation method	Superiorly CO-tolerant	Cost of pd precursor	
CuNi	35.1	-	Chemical reduction	-easily recollected from the reaction system by an external magnetic field due to their considerable saturation magnetization	The higher oxygen affinity of Ni.	Jinglei *et al* ., 2014

2.3. Carbon Based Materials for Electrocatalysis of Methanol

The electrocatalytic activity can be enhanced by increasing the surface area through dispersion of catalysts on suitable support material and hence lowering the precious metal loading content. Some of the main properties required for practical supports that can be used with oxygen reduction electro catalysts are: Acceptable electronic conductivity, adequate chemical or electrochemical stability in the electrolyte environment and the ease of fabrication into electrode structures (Asanda, 2010).

Carbon black was the typical catalyst support material of choice for MFC applications. There were various types of carbon support materials including the conventional carbon black, nanostructured carbon such as carbon nanotubes and carbon nanofibers, mesoporous carbon, nano-diamonds and doped diamonds, as well as graphene. The carbon support boasts of essential fuel cell properties such as: high surface area, high electrical conductivity compared to other supporting material, well-developed pore structure, as well as availability and cost effectiveness of the carbon material. Unfortunately, with all those outstanding advantages, carbon support suffers from electrochemical instability in the fuel cell environment which was a major drawback in using them as support materials (Takasu *et al.*, 2000).

2.3.1. Carbon Nanotubes

Carbon nanotubes have stimulated a great interest for several applications, including hydrogen storage, field emission, super-conductivity and heterogeneous catalysis. The unique structural, mechanical and electrical properties of CNTs have made them to be proposed as a replacement for traditional carbon black, as an alternative support for fuel cell catalysts. Carbon nanotubes consist of rolled up graphene hexagonal sp^2 carbon layer, which forms cylinders with diameters of nanometer sizes and length of up to millimeters. They are synthesized as single wall carbon nanotubes (SWCNT) or multi-walled carbon nanotubes (MWCNT) (Gao *et al.*, 2009). Therefore, CNT have been investigated as advanced electrocatalyst support due to their distinctive electrochemical characteristics

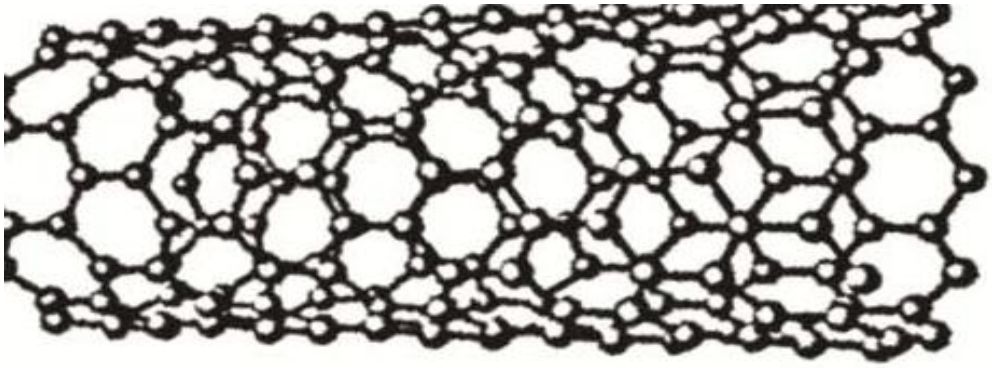

Figure 3 .Carbon nanotubes structure

2.3.2. Graphite

An allotropic form of the element carbon consisting of layers of hexagonally arranged carbon atoms in a planar condensed ring system. The layers are stacked parallel to each other in a three-dimensional crystalline long-range order. There were two allotropic forms with different stacking arrangements, hexagonal and rhombohedral. The chemical bonds within the layers were covalent with sp^2 hybridization and with a C-C distance of 141.7 pm. The weak bonds between the layers were metallic with strength comparable to van der Waals bonding only. Thus, graphite composite is chosen as a novel electrode system for mediating the metal catalytic electro-oxidation of methanol (Schedin *et al*., 2007).

2.3.3. Graphene

Graphene consists of a layer of sp^2 carbon hexagonal networks, in which strong covalent bonds were formed between two adjacent carbon atoms. In the graphene lattice, two sub-lattice of carbon atoms are bonded together with σ bonds, and π orbital of each carbon atom in the lattice contribute to a delocalized network of electrons. The electronic structure of graphene is different from typical 3D materials. Exactly one layer of a polycyclic aromatic hydrocarbon network, with all carbon atoms hexagonally arranged in a planar condensed ring system. It has a metallic character and consists solely of carbon and hydrogen. (Bong *et al*., 2010). Besides the superior electrical conductivity and outstanding mechanical properties, as a

one-carbon atom-thick material, graphene has a high surface-to-volume ratio and a theoretical mass-specific surface area up to 2630-2965 m^2/g. This surface-to-mass ratio is much larger than that of other carbon materials such as CNTs, carbon black, etc (Ozkan *et al.*, 2010). Therefore, graphene has a unique advantage as a supporting platform for use of catalytic metallic materials to electro-oxidize methanol compared to other nonmaterials such as carbon black, CNTs, carbon nanofibers (CNFs) and etc (Lei *et al*., 2010).

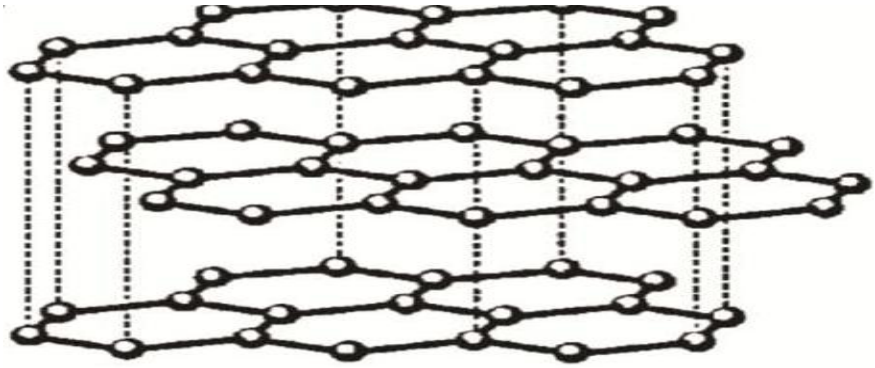

Figure 4. Graphite structure

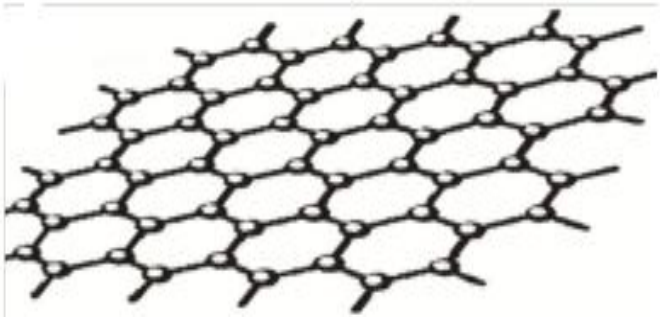

Figure 5. Graphene structure

2.3.4. Reduced Graphene Oxide

Reduced graphene oxide (RGO) or graphene nano sheets, single layers of carbon atoms tightly packed into 2-dimensional (2D) honeycomb sp^2 carbon lattices, have received much attention in the past few years (Ishigami *et al*., 2007; Kim *et al*., 2 010). Apart from its unique electronic

properties (Geim and Novoselov, 2007), RGO has several other excellent attributes, such as the large theoretical specific surface area and good chemical stability (Loh *et al*., 2010). The excellent electrical conductivity along with thermal conductivity, high surface area (theoretically 2630 m^2/g for single-layer graphene) and strong mechanical strength make the RGO useful in many applications, including electronics ,solar cells ,fuel cells as well as energy storage and conversion devices, such as super capacitors and batteries (Liu, 2014). Different from the brittle graphite, RGO sheets are flexible, which is an advantage for fabrication of flexible electronic and energy storage devices. Especially, RGO has potential application as a heterogeneous catalyst support in methanol fuel cells (Eda *et al*., 2008).

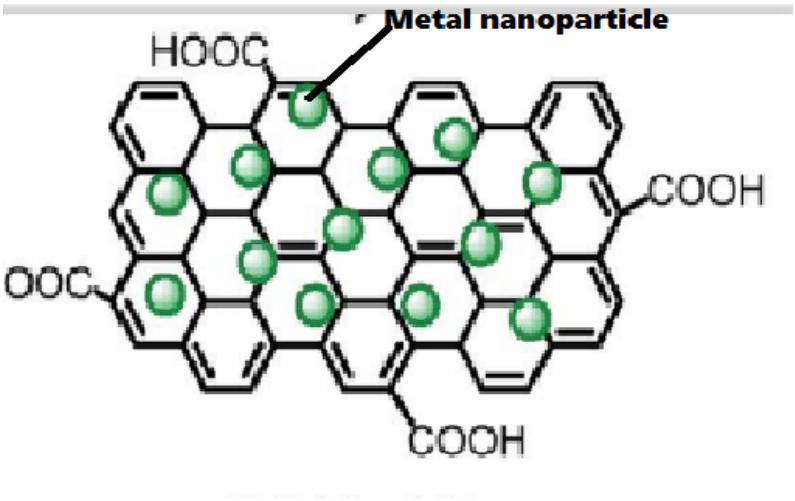

Figure 6. Schematic illustration of the metal nanoparticles reduced graphene oxide

2.4. Synthesis of Monometallic and Bimetallic Nanoparticles

Both bimetallic and monometallic nanoparticle can be prepared by different methods. Metal nanoparticle can be prepared by two ways by subdivision of bulk metals (a physical method) and growth of particle from molecular or ionic precursors (chemical method) (Nilendri, 2014). The chemical method was more suitable than that of the physical methods as the size and uniformity of the metal nanoparticles can be controlled by the chemical method. Nanoparticle synthesized by physical method has broad particle size distribution typically particle size greater than 10 nm with distribution greater than 20 percent (Nilendri, 2014). Basically there were two approaches for nanoparticle synthesis top-down and bottom-up. The top-down

approach involves the breaking down of the bulk material into nano sized structures or particles. These approaches were inherently simpler and depend either on removal or division of bulk material or on miniaturization of bulk fabrication processes to produce the desired structure with appropriate properties. The biggest problem of this approach was that it introduces internal stress, surface defects and contaminations (Nilendri, 2014).While Bottom up approaches adopt molecular components that were built up into more complex assembly, and many of these techniques were still under development or were just beginning to be used for commercial production of nanopowders. Some of the most common preparation methods of nanoparticles are:

- The colloidal method of preparation
- The microemulsion method of preparation
- The chemical reduction method of preparation
- The electrochemical reduction method of preparation
- The impregnation method of preparation

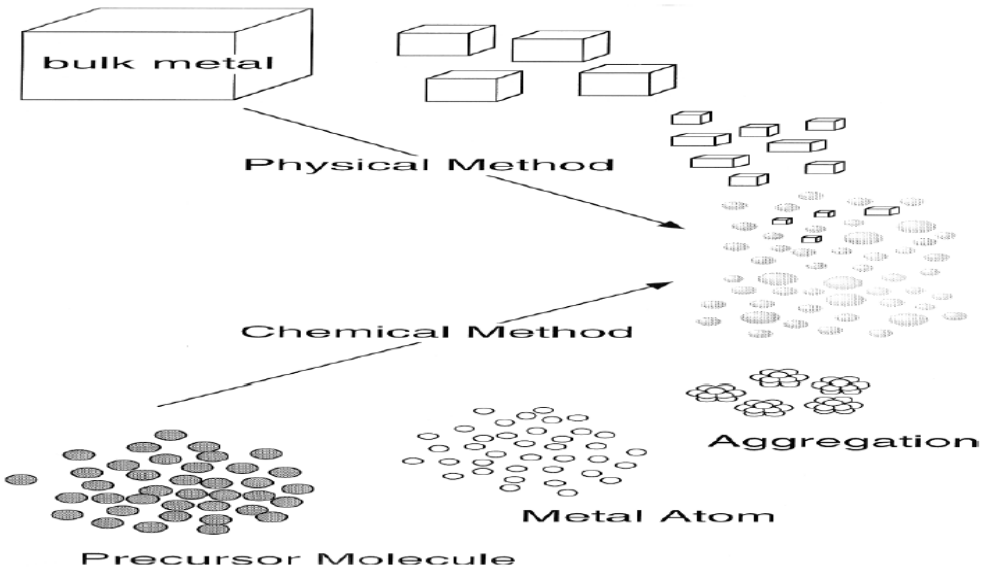

Figure 7**.** Schematic illustration of preparative methods of metal nanoparticles

2.4.1. The Colloidal Method of Preparation

This was employed extensively explored for preparation of Pt nanoparticle (Tang *et al.*, 2004). Includes the following common steps: 1) preparation of Cu containing colloids; 2) deposition of the colloids onto the support; and 3) chemical reduction of the mixture. Other colloid methods using several reducing agents, organic stabilizers or shell-removing approaches have also been developed in recent years. The colloidal method using ethylene glycol (EG) as a reducing agent and solvent was employed in this work as a method of synthesis for PtRu and PtSn electro catalysts (Roustom *et al*., 2007).

2.4.2. The Microemulsion Method of Preparation

By this method, a better control of particle size, shape, size distribution, and chemical composition are possible, although a number of techniques have been used for producing nanoparticles which include gas evaporation sol–gel methods sputtering and co-precipitation (Zhang and Chan 2003) .The microemulsion is a nanoscaled aqueous liquid droplet containing a noble metal precursor. The droplets are engulfed by surfactant molecules and uniformly in an immiscibly continuous organic phase. The first step in this method is the formation of Pt nanoparticles through water-in-oil microemulsion reaction, followed by a reduction step. The microemulsion here serves as a nanoscaled reactor in which the chemical reactions take place. The reduction step can be carried out by either adding a reducing agent (e.g., N_2H_4, HCHO, and $NaBH_4$) into the microemulsion system, or by mixing it with another reducing agent-containing microemulsion system. As a result the reaction is kept into the inside of the nanoscale microemulsion, and the formed particle sizes can be easily controlled by the magnitude of the microemulsion size. The removal of surfactant molecules can be easily carried out by heat-treating the high surface area carbon support nanoparticles. The main advantage of the microemulsion method is its ease in controlling metallic composition and particle size within a narrow distribution by varying the synthetic conditions, however, using this method is expensive as it uses costly surfactants molecules and another drawback to employing the microemulsion method is that it requires a number of separation and washing steps, which may be suitable for large-scale production (Zhang and Chan 2002).

2.4.3. Chemical Reduction

In this method, metal ions are reduced to zero valent state and co-ordination of stabilizing polymer to metal nanoparticles. In practice, reduction can be precedes or followed by the interaction between metallic species and polymers. If the reduction precede the interaction, the structural properties of thermal nanoparticles are determined only by the reduction condition but if the interaction precede the reduction, the interactive force between polymers and metal ions may affect the size and structure of metal nanoparticle .$NaBH_4$ or KBH_4 reduction methods have been widely used for the synthesis of Au, Ag, Pt, Pd, Ni and Cu nanoparticles. Advantages: i) the method was very simple and reproducible, ii) particle size of the obtained metal nanoparticles was small with a narrow size distribution, iii) size of particle can be controlled by altering the preparative condition such as varying the concentration of metals, etc., iv) the obtained colloidal dispersion of metal nanoparticle show a high catalytic activity, and v) the obtained colloidal dispersion are stable and no precipitates normally observed for years (Nilendri, 2014).

2.4.4. The Electrochemical Method

The electrochemical method can be used to generate metal atoms from the bulk metal by electrodeposition at liquid-liquid interfaces. An electrochemical method was proposed to oxidise the bulk metal and reduces the metal ions to prepare nanoparticles stabilized by tetraalkylammonium salt, with particle size selectivity controlled by the current density. An electrolytic cell set up consists of two metal electrodes of the bulk metals from which atoms are created to form the nanoparticle. Bimetallic nanoparticles such as Pd-Pt, Ni-Pd, Fe-Co, Ni-Cu and Fe-Ni can be prepared electrochemically. This involves inserting metal plates of the two bulk metals into an electrolyte, which both serve as anodes. The electrolyte contains a salt of tetraalkylammonium which acts as a stabilizer. The cathode was a platinum plate (Andisiwe, 2013). The metal ions were oxidized to their corresponding ions at the anode, and the Pt cathode produces electrons. The metal ions were then reduced by these electrons to the metal atoms, which aggregate to form the bimetallic nanoparticles, which were stabilized from further aggregation by the tetraalkylammonium salt in the electrolyte.

2.4.5. The Impregnation Method of Preparation

The impregnation method is characterized by a deposition step of Pt or other metal precursors followed by a reduction step. Deposition means soaking up of a dissolved metal precursor, e.g. $PtCl_6^{2-}$ into the pores of a support, e.g. Vulcan 72 carbon, before reduction of the metal precursor to metal nanoparticles. This method is simple and has been the most common method used for electrocatalyst preparation over the years. The reduction step can be chemical or electrochemical. The chemical reduction may be (liquid-phase reduction) (Park *et al.*, 2003) of the metallic catalysts slurry in solution by using reducing agents or gas phase reduction of the metallic particles impregnated carbon using a flowing H_2 gas stream at a rather high temperature of about 250–600 ^{0}C (Arico *et al.* 2004). The common reducing chemicals are hydrazine, borohydride, formic acid, and hydrogen. Borohydride are mostly used for the reduction. In the case of hydrogen, temperature elevation to above 300 ^{0}C under an inert atmosphere is required. The major drawback of the impregnation method is the lack of size control of metal particles except when the porous substrate has a narrow pore size distribution, e.g. in highly ordered mesoporous carbon (Li *et al*., 2005).

2.5. Physical Characterization Methods

2.5.1. X-Ray Diffractometry

X-ray diffraction is a rapid technique that gives information about the structure of the solid materials, the arrangement of atoms that compose the solid sample and crystallinity of the sample. It is widely used because of it permits nondestructive structure characterization and is extensively used acquire qualitative, quantitative, crystallinity, residual stress and crystallite size information of solid samples. In this study XRD is used to investigate the atomic structure, particle size and lattice parameter of the electro catalysts and the support material. Bragg's law (equation 2.1) below, which relates the wavelength of electromagnetic radiation to diffraction angle and the lattice spacing in a crystalline sample.

$$n\lambda = 2d\sin\theta \qquad (2.1)$$

The degree of crystallinity of the sample can be measured by the width of the peak in a diffraction pattern associated with a particular planer reflection from within the crystal unit cell. The larger the peak area the more amorphous the sample is and if the area under the peak is narrow, the sample is more crystalline. XRD can also be used quantitatively to elucidate the particle size using the Scherrer equation, given as:

$$D = 0.9\lambda / \beta\cos\theta \qquad (2.2)$$

Where D = particle size, 0.9 =shape factor, λ = x-ray wave length, β =peak –width at half-height (radians), θ = angle of reflection.

In addition to the information provided, the lattice parameter (α) can be calculated by the following equation:

$$a_0 = d\,(h^2 + k^2 + l^2)^{1/2} \qquad (2.3)$$

Where h, k, and l constitute the Miller indices of a crystal facet, and d is the interplanar spacing determined using Braggs‟ Law (Danafar *et al*., 2009).

2.5.2. Scanning Electron Microscopy (SEM)

Scanning electron microscopy is an imaging technique used in all fields that require characterization of solid materials, with the ability of producing profiles of material surfaces. It permits the observation and characterization of heterogeneous organic and inorganic materials on a nanometer (nm) to a micrometer (μm) scale. SEM is used to provide information about the surface morphology, particle size and appearance of supporting material and electro catalysts.

2.5.3. Fourier Transform Infrared Spectroscopy (FTIR)

FT-IR is one of the techniques that are used today for measuring the intensity of infrared radiation as a function of frequency or wavelength. When an infrared light interacts with the

sample, chemical bonds will stretch, contract and bend. As a result, a molecular fingerprint of the sample can be produced as the chemical functional group tends to absorb infrared radiation in a specific wave number range regardless of the structure of the rest of the molecule, which makes infrared spectroscopy useful for several types of analysis (Liu, 2014).

2.5.4. Ultraviolet–visible Spectroscopy

A typical UV-Vis spectroscopic analysis consists of measuring the wavelength dependence of the light transmitted through the sample .When the light passes through or is reflected from the sample, the amount of light absorbed is the difference between the incident and the transmitted radiation. A classical semiconductor exhibits minimal optical absorption or high absorption for photons when energies are smaller or greater than the band gap. As a result, there is a sharp increase in absorption at energies close to the band gap resulting in absorption edge /reflection threshold in the UV-Vis absorbance spectrum. According to Tauc, the dependence of the absorption coefficient α on the photon energy hν for near- edge optical absorption in semiconductors takes the form $(\alpha h\nu)^{1/m} = k(h\nu - E_g)$ where E_g is the optical band gap, k is a constant and m=1/2 for an allowed direct energy gap and m=3/2 for a forbidden direct energy gap. In order to determine the optical band gap of a semiconductor thin film, taking m=1/2, $(\alpha h\nu)^2$ must be plotted versus hν using the data obtained from the optical absorption spectra. The direct band gap of the semiconductor thin film is obtained by extrapolating the linear part to the zero of the ordinate (Liu, 2014).

2.6. Electrochemical Methods

2.6.1. Linear Sweep Voltammetry

Linear sweep voltammetry (LSV) differs from CV in that the applied potential is swept at a fixed sweep rate from an initial potential to a final potential and there is no back and forth. LSV was used in this study to investigate the oxygen reduction reaction and methanol oxidation reaction (Ocampo *et al.*, 2006).

2.6.2. Cyclic Voltammetry (CV)

Cyclic voltammetry (CV) was a type of potential-controlled electrochemical technique, which can be used to examine the electrodes surface reactions, the behavior of the electrochemically-active species, and to investigate the quality of electrocatalyst (Yoo *et al.,* 2009). Cyclic voltammetry provides information on the thermodynamics of redox processes and kinetics of heterogeneous electron transfer reactions. A few drops of the modifier solution (Drop-dry coating) were applied onto the electrode surface and left to stand to allow the solvent to dry out.

The potential of the working electrode is swept linearly with time and between two potential ends. By adjusting the potential of the working electrode, electrons are transferred between the electrode and the molecules in the electrolyte, which records the current response of the working electrode when the potential is swept back and forth between two selected potentials .Cyclic voltammetry was used in this study to examine the electrocatalytic surface area (ECSA) and durability of nanophase supported electrocatalyst The three-electrode method was the most widely used because the electrical potential of reference does not change easily during the measurement. This method uses a reference electrode (RE), working electrode (WE), and counter electrode (CE) (also called the secondary or auxiliary electrode). Standard CV experiments consist of measuring the current flowing through the wire during a triangular potential perturbation. The applied potential is measured against the RE, while the CE closes the electrical circuit for the current to flow. The experiments are performed by a potentiostat that effectively controls the voltage between the RE and WE, while measuring the current through the CE the WE was connected to the ground (Isidorsson et al., 1996). Electrolyte was usually added to the test solution to ensure sufficient conductivity. The combination of the solvent, electrolyte and specific working electrode material determines the range of the potential to be applied.

Cyclic voltammetry can be considered as a reversal technique, which involves sweeping the electrode potential between two limits at a known sweep rate. At the beginning the working electrode was held at some potential, Ei, where no electrode reactions occur. During

the change of the potential (when the oxidized form, O) from E1 to E2 (in negative direction), a cathodic current begins to increase, until a peak is reached (Fig.8a). After traversing the potential region in which the reduction process take place, of the potential sweep is reversed. During the reverse scan, R molecules (generated in the forward half cycle, and accumulate near the surface) are deoxidized back to O and the anodic peak. In the reversible systems the position of the peaks on the potential axis (Ep) is related to the formal potential of the redox process. The formal potential for a reversible couple is centered between the anodic peak potentials (Ep,a) and the cathodic peak potentials (Ep,c). A theoretical cyclic voltammogram for a reversible system is shown in Fig.8b. For the Cathodic scan (applied potential is decreasing) the current has a negative sign, for the anodic scan (applied potential is increasing) the current has a positive sign.

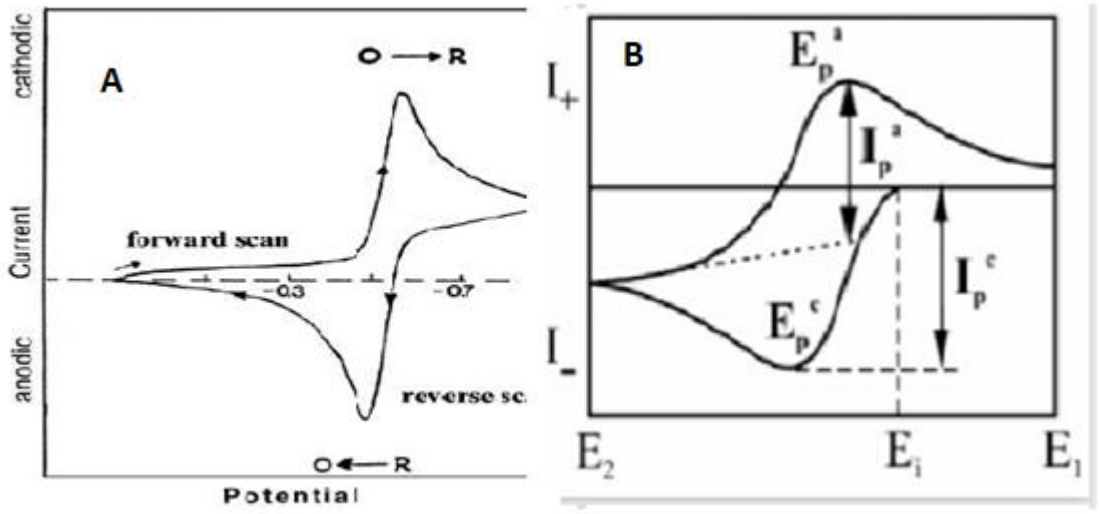

Figure 8. A) Typical cyclic voltammogram for a reversible O + ne- ↔ R redox process B) A reversible reaction; anodic (a) and cathodic (c) processes, Ep was the potential at the peak current Ip

2.6.3. Chronoamperometry

Chronoamperometry involves stepping the potential of the working electrode from a value at which no faradaic reaction occurs to a potential at which the surface area concentration of the electroactive species is effectively zero (Cheng *et al.*, 2007). The resulting current – time

dependence is monitored. Even though the chronoamperometry is relatively simple technique, there are a number of difficulties, which are related to the interpretation of the current-transient curve. Hence, it is very important to find the possibility of comparative analysis of the chronoamperometry results with the results of cyclic voltammetry and other techniques.

2.6.4. Electrochemical Impedance Spectroscopy (EIS)

EIS records the response from an electrochemical system by the stimulation of an imposed periodic small amplitude AC signal (Zhou *et al*., 2013). Impedance is a measure of the circuit characteristics to impede the flow of electrons through the circuit. The basic Ohm's law in Eq. 2.6 defines the resistance R in term potential, E, and current I (Bard and Faulkner, 2001).

$$\mathbf{R = \frac{E}{I}} \qquad \mathbf{2.6}$$

The excitation signal can be expressed as a function of time

$$\mathbf{E_t = E_0 \sin \omega t} \qquad \mathbf{2.7}$$

where E_t is the potential difference at time t, E_0 is the amplitude of the voltage signal at t = 0, and ω is the angular frequency given by ($\omega = 2\pi f$) expressed in radians/second and frequency, f, in hertz. The rate of an electrochemical reaction can be strongly influenced by diffusion of reactants towards, or away from the electrode-electrolyte interface. This situation can exist when the electrode is covered with adsorbed solution components or a selective coating. Nyquist plot also known as Cole-Cole plot is one of the most critical and popular formats for evaluating electrochemical parameters like electrolytic solution resistance (Rs), electrode polarization resistance (Rp) and double layer capacitance (Cdl), etc (Bard and Faulkner, 2001).

The solution resistance (Rs) is the resistance between the working electrode and the reference electrode. The solution resistance is not usually calculated, it is given when fitting the impedance data to a corresponding circuit. High-frequency intercept lies closer to the origin of the plot .In Fig.9 it could be read as 25 kΩ. The real axis value at the other (low frequency)

intercept is the sum of solution and polarization resistance. The low-frequency intercept could be read by interpolating the semi-circle to the real axis. In Fig.9 it reads as 325 kΩ).The charge transfer resistance (Rct) associated with the charge transfer mechanism for electrode reaction, obtained by reading the real value at low frequency intercept of real values (Olson and Buhlmann, 2010).

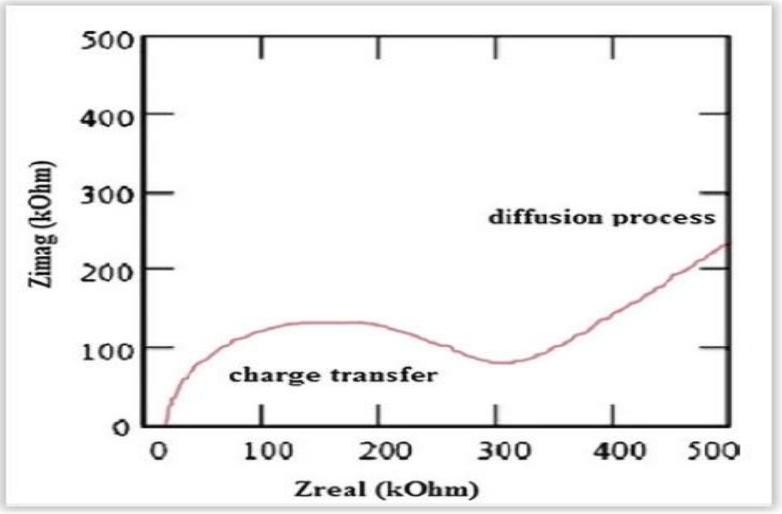

Figure 9. Nyquist plot for Randle's electrochemical cell model

3. MATERIALS AND METHODS

3.1. Experimental Site

The synthesis of nanoparticles, Cu-RGO, Ni-RGO and Ni-Cu/RGO, Cyclic Voltamography (CV) electrocatalytic activity, Ultraviolet–visible spectroscopy (Uv–vis) study was conducted at Haramaya University Research Laboratory. Characterizations with X-Ray Diffractometry (XRD) and Fourier Transform Infrared spectrometer (FTIR) were conducted at Addis Ababa University, Chemistry Department. Scanning Electron Microscopy (SEM) and Energy-Dispersive Spectrum (EDX) were conducted in Addis Ababa Leather Industry Development Institute.

3.2. Apparatus and Equipment

During synthesis and characterization of the as-synthesized electrocatalytic nanoparticles, the following materials and equipment were used: Uv-visible spectrophotometer (SANYO, SP65), X-ray Diffractometry (RIGAKU Miniflex 600, Japan), Scanning Electron Microscopy (JSM-IT300), Infrared, Spectrum 65 FTIR (Perkin-Elmer), Cyclic Voltammetry (CV), Linear Sweep Voltammetry (LSV), Chronoamperometry (CA) and Electrochemical Impedance Spectroscopy (EIS) were carried out using BAS 100B Electrochemical Bioanalyzer (BAS100B). Platinum electrode (0.02 cm^2) was employed as a working electrode; a platinum wire and Ag/AgCl (saturated 3M KCl) were used as counter and reference electrodes, respectively. pH meter, reactor tube, oven (Contherm 260 M), analytical balance (OHAUS, made in Switzerland), hot plate (SM 6, made in U.K), deionizer, furnace, centrifuge (K_2 series, CENTERION SCIENTIFIC LTD, made in West Sussex.U.K were used.

3.3. Reagents and Chemicals

Methanol (CH_3OH, 99.5%), nickel chloride hexahydrate ($NiCl_2.6H_2O$, Merck India), Sodium hydroxide (NaOH, 98%), hydrochloric acid (HCl,37% , qualigens, India), sulfuric acid (H_2SO_4 97-98%, Qualigens, India), reduced graphene oxide (Sigma-Aldrich), copper chloride hydrate ($CuCl_2.2H_2O$, Sigma-Aldrich), poly ethylene glycol, hydrazine hydrate ($N_2H_4.H_2O$), KCl (Merck Germany), Alumina polishing powders (0.05µm), potassium ferricyanide ($K_3Fe(CN)_6$, 95%, Merck, Germany), and Ethanol (76%) used in this study were all analytical reagent grade and used without further purification.

3.4. Synthesis Methods

3.4.1. Synthesis of Cu-RGO

The Cu-RGO nanocomposite was prepared by chemical reduction method. 3.69 g of copper chloride hydrate ($CuCl_2{\cdot}2H_2O$) in 100 mL of deionized water was dissolved. This step was followed by addition of 99 mL of PEG, which act as capping agent under continuous magnetic stirring at 60 ℃ for 30 minutes until the formation of color. Furthermore, under a continuous stirring for 30 minutes. Then 24 mL of hydrazine was slowly added till the color of the suspension was changed to red-brown (Khalid *et al..*, 2015). The pH of the solution was adjusted to 10.5 by adding drop-wise suitable amounts of 1 M NaOH to maintain the alkalinity during the course of reaction (Ankur and Manivannan, 2015). In a separate volumetric flask, 2 mg of RGO was mixed with 10 mL of ethanol and ultrasonicated for about 1h. After the RGO solution was added to Cu NPs solution. The mixture was continuously stirred under nitrogen gas at 60 ℃ for 2 h. Brownish-black color was observed showing the formation of Cu-RGO nanocomposite (Ankur and Manivannan, 2015). In the next step, the precipitate was collected and repeatedly washed with DI water and ethanol to remove the impurities. Finally, the product (Cu-RGO) was vacuum dried at100 ℃ for 2 h (Rahul *et al.*, 2016).

3.4.2. Synthesis of Ni-RGO

The Ni-RGO nanocomposite was produced using the same procedure as Cu-RGO. 3.69 g of nickel chloride hexahydrate ($NiCl_2.6H_2O$) dissolved in 100 mL of deionized water. This step was followed by addition of 99 mL of PEG, which act as capping agent under continuous magnetic stirring at 60 ℃ for 30 minutes. The stirring continued till the solution changes to blue color. Then 24 mL of hydrazine hydrate was slowly added to the above solution and stirred for 1h, the color of the suspension is changed to black color indicating the formation of nickel nanoparticles (Man deep *et al.*, 2011). The pH of the solution was adjusted at pH (~8) which is favorable to form nickel nanoparticles by adding drop-wise suitable amounts of 1 M NaOH (Jeer pan *et al.*, 2014). To form Ni-RGO nanocomposite 2 mg of RGO was mixed with 10 mL of ethanol and ultrasonicated for 1h. The RGO solution was added to Ni NPs solution. Then the mixture was continuously stirred under nitrogen gas at 60 ℃ for 2 h to confirm the formation of black color. The black precipitate was collected and repeatedly washed with DI water and ethanol to remove the impurities. Finally, the Ni-RGO product was vacuum dried at100 ℃ for 2 h (Zhigang *et al.*, 2012).

3.4.3. Synthesis of Ni-Cu/RGO

A Ni-Cu bimetallic nanoparticle has been prepared by hydrazine reduction method using ethylene glycol (Moganavally *et al*., 2014). 3.6 g of $CuCl_2.2H_2O$ and 8.4 g of $NiCl_2.6H_2O$ in the molar ratio of (30:70) were dissolved in 100 mL of deionized water. This step was followed by addition of 99 mL of PEG, which act as capping agent under continuous magnetic stirring at 60 ℃ for 1h till a blue color appeared in the solution. Furthermore, 50 mL of hydrazine hydrate was slowly added under a continuous stirring for 1h. The pH of the solution was adjusted at pH ~8 by adding drop-wise 1.8 mL of 1 M NaOH (Jinglei *et al.*, 2014). The reduction reactions could be expressed as

$$2Ni^{2+} + N_2H_4 + 4OH^- \longrightarrow 2Ni + N_2 + 4H_2O \text{ and}$$

$$2Cu^{2+} + N_2H_4 + 4OH^- \longrightarrow 2Cu + N_2 + 4H_2O$$

To produce Ni-Cu/RGO nanocomposite; 6 mg of RGO was mixed with 25 mL of ethanol and ultrasonicated for 1:30 h, the RGO solution was added to Ni-Cu NCs solution. Then the

mixture was continuously stirred under nitrogen gas at 60 ℃ for 2 h (Rahul *et al*.., 2016). The precipitate was collected and repeatedly washed with DI water and ethanol to remove the impurities. Finally, the product was vacuum dried at100 ℃ for 2 h and referred as Ni-Cu/RGO (Rahul *et al*., 2016).

3.5. Characterization of the as Synthesized Nanocomposites

Powder x-ray diffraction (XRD, CuK_{α} radiation of wave length; λ=1.54 nm with scan rate of $0.12^{0}min^{-1}$, at 2θ range of (10-80) was used to characterize crystallinity of Cu-RGO, Ni-RGO and Ni-Cu/RGO nanocomposites to be employed as electrocatalyst for methanol oxidation). The uv-visible spectra measured by using a SANYO, SP65 spectrophotometer between 200 and 800 nm wavelength regions. FTIR spectroscopy measured on spectrum 65 FTIR (Perkin Elmer) in the range 4000-400 cm^{-1} was used to determine the functional groups of the as synthesized nanomaterials. The morphology of the Cu-RGO, Ni-RGO and Ni-Cu/RGO materials was characterized using SEM (JSM-IT300) scanning electron micro analyzer with an accelerating voltage of 20.0 kV. EDX analysis was performed to determine the elemental composition of the particles using Oxford - Energy Dispersive X-ray system (IT300, LA).

3.6. Electrochemical Characterization of the as Synthesized Nanocomposites

Electrochemical characterization of the as synthesized nanocomposites was performed by employing Bas 100B Electrochemical Analyzer in a conventional three electrode arrangement using platinum (a geometric area of 0.02 cm^2) modified by Cu-RGO, Ni-RGO and Ni-Cu/RGO as a working electrode and a silver/silver chloride (saturated KCl) and a Pt wire were used as the reference and auxiliary electrodes, respectively. Prior to modification, the bare electrode was successively polished with 0.05 μm α-Al_2O_3 power slurries until a shiny mirror-like surface was achieved, followed by ultrasonication in 1:1 ethanol and deionized water for 5 min and dried at room temperature in a desicator for 1h. The catalyst slurry was prepared by mixing 6 mg of the Cu-RGO composite powder in a mixture of 2 mL ethanol and about 2 μL Chitosan solution (chitosan solution (2 mg/mL) was prepared in 1% acetic acid solution

(Mehri *et al*., 2016)) under ultrasonication for 40 min to form a homogeneous black suspension. About 20 μL of the electrocatalyst suspension was carefully coated onto the surface of the platinum electrode and air-dried before performing the electrochemical measurements (Ruimin *et al*., 2011). The Ni-RGO and Ni-Cu/RGO modified Pt electrode was prepared using the same procedure. The electrochemical oxidation of methanol using cyclic voltammetry was carried out in aqueous 0.1M NaOH solution in potential range from -0.1 to 0.6 V at scan rate of 10 to 100 mV/s. (The effect of methanol concentration (0.1 to 2.0 M) on the performance of Ni-Cu/RGO electrocatalyst was studied using linear sweep voltammetry in 0.1 M NaOH at scan rate of 50 mV/s in the potential range from -0.1 to 1.2 V.

The stability of the electrocatalyst was investigated using chronoamperometry (CA) in a solution of 0.1 M NaOH containing 0.1M CH_3OH for 300 s at 0.47 V vs. Ag/AgCl (saturated KCl) (Ezhil *et al.,* 2016). Besides, the as synthesized nanomaterials were characterized using electrochemical impedance spectroscopy (EIS) using 100B BUS impedance model using DC voltage 0.5 V and 5 mV amplitude of the alternative voltage in the frequency range from 1000 Hz to 0.1 Hz

4. RESULTS AND DISCUSSION

4.1. Physical Characterization

4.1.1. X-Ray Diffraction Analysis

The XRD patterns of Cu-RGO, Ni-RGO and Ni-Cu/RGO nanocomposites are shown in Fig. 10.The successful formation of Cu and Ni monometallic NPs, and Ni-Cu bimetallic NPs, along with RGO is confirmed from XRD analysis. As seen in Fig. 10 (a) the diffraction peaks at 2θ value of 43.7°, 50.84° and 74.9° corresponding to (111), (200), and (220) planes respectively, belong to the face centered cubic structure of Cu (JCPDS No.96-410-5041). Our findings are similar with previous reports (Gitashree *et al.,* 2017). The diffraction peak at 2θ value of 29.1° could be indexed to cuprous oxide (Cu_2O) (appendix Fig.1a). The presence of Cu_2O indicates the partial oxidation of copper nanoparticles with dissolved oxygen in the solution (Hina *et al.,* 2015). On the other hand Fig.10 (b) the diffraction peaks shown at 2θ = 44.68°, 51.98° and76.54° corresponding to the crystallographic diffraction planes of (111), (2 0 0) and (2 2 0) are attributed to face centered cubic structure of Ni (JCPDS No.96-901-2973) and the highest intense diffraction peak at around 44.68° suggests the well crystalline nature of Ni-NPs (Rahul *et al.,* 2016).

According to the literature, Ni and Cu elements have similar electronic structure and atomic radii. Therefore, they can easily form similar cubic structures (Wang *et al.,* 2012). The XRD pattern of the bimetallic deposited reduced graphene oxide (ternary system) shown in Fig.10 (c) revealed the presence of both metals: Cu at 2θ values of 43.76°, 50.84° and 74.92° Cu (JCPDS No.96-410-5041) and Ni at 2θ values of 44.84°, 52° and 76.64° Ni (JCPDS No.96-901-1604), showing that the precursors are completely converted into Ni-Cu alloy nanoparticles, which suggests the formation of a Ni-Cu solid solution of bimetallic nanoparticles. All the peaks correspond to Ni-Cu alloys with a face-centered cubic crystalline structure (Garci *et al*., 2011; Arul *et al*., 2014; Rahul *et al.,* 2016).

The XRD patterns of GO exhibits a sharp peak at around 10.9° (Rahul *et al.*, 2016). After the reduction and intercalation of metal NPs with graphene this peak was completely diminished and new diffraction peaks of Cu-RGO, Ni-RGO and Ni-Cu/RGO at 2θ values around 22.9°, 23.32° and 23.43°, respectively, suggest the successful formation of RGO nanospheres during nanocomposite formation. Since the particle size and particle morphology greatly influence the electrochemical activity of the catalyst owing to the relationship between catalytic activity and surface structure, the average particle size and lattice parameter were collected and presented in table 3 below. The estimated average particle size is found to be around 11.94, 8.86 and 6.83 nm for Cu-RGO, Ni-RGO and Ni-Cu/RGO respectively indicating the formation of small crystals via chemical reduction method. Therefore, the bimetallic works with synergism and provides the extra defect sites for reactions by increment of catalytic surface area.

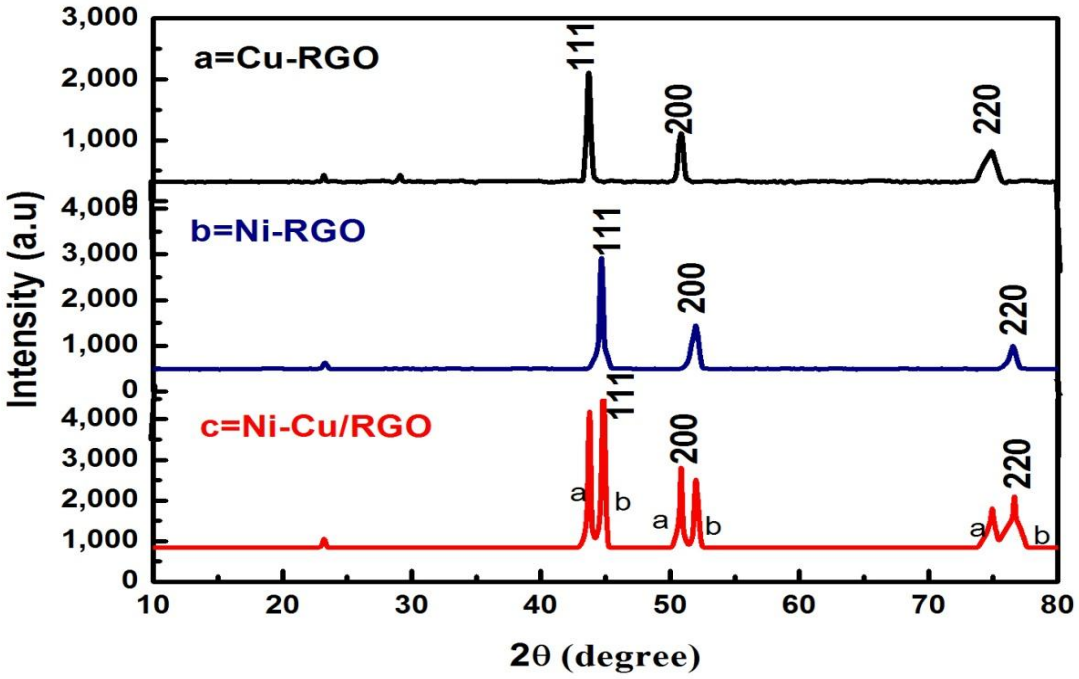

Figure 10. XRD pattern of Cu-RGO, Ni-RGO and Ni-Cu/RGO nanocomposite

The average crystallite size of the as-synthesized ternary nanocomposite was compared with ternary nanocomposite synthesized more or less in similar approach by Rahul *et al.*, (2016). The crystal size of our nanocomposite (6.8 nm) is found to be smaller than the reported literature value (12.7 nm). It is also noted that the presence of RGO resulted to smaller crystallite size. For example, binary Cu-Ni nanoparticles produced by rapid microwave combustion method (Arul *et al*., 2014), obtained average crystallite size around 33.25 nm. Therefore, the presence of RGO in the binary metallic mixture could result to smaller crystallite size nanomaterials with anticipated better specific surface area that helps expedite the catalytic reaction, such as methanol oxidation.

Table 3.Calculated particle size, d-spacing and lattice parameter

Composites	2θ	FCC (hkl)	d(nm) = 0.154 nm/2sinθ	β (radian)	D(nm) = 0.9λ / βcos θ	$a_{0(nm)=}$ $d(h^2+k^2+l^2)^{1/2}$
Cu-RGO	43.7	111	0.207	0.016	11.94	0.358
	50.84	200	0.179			0.359
	74.9	220	0.127			0.358
Ni-RGO	44.68	111	0.203	0.022	8.86	0.351
	51.98	200	0.176			0.351
	76.54	220	0.124			0.352
Ni-Cu/RGO	44.84	111	0.201	0.029	6.83	0.35
	50.84	200	0.179			0.359
	76.64	220	0.124			0.351

4.1.2. FTIR Analysis

FTIR analysis was used to examine the chemical composition of the materials (Fig.11). The intensity of the stretching bands of oxygen functionalities like O- H and C= O (3389 and 1733 cm^{-1}, respectively) are greatly reduced in the nanocomposites when compared to GO reported, indicating successful formation of metal nanoparticle reduced graphene oxide composites (Dreyer *et al.,* 2010 ; Gitashree et al., 2017). Bands observed at 3437 cm^{-1}, 3414 cm^{-1} and 3401

cm^{-1} correspond to O-H stretching bands due to adsorbed water molecules onto the nanocomposite for Ni-RGO, Cu-RGO and Ni-Cu/RGO respectively. This decrease in wave number may occur due to interaction of Cu NPs, Ni NPs and Cu-Ni NCs with RGO group. The absorption bands observed at 2923 and 2871 cm^{-1}could be attributed to C–H stretching (Gitashree *et al*., 2017). The bands in the region 2000-1500 cm^{-1} are due to C=C bond or H-O-H bending vibrations. This bond appears at 1631 cm^{-1} and 1597 cm^{-1} and shifted to 1606 cm^{-1} after ternary nanocomposite formation. The shifting in wave numbers might be due to the C=C stretching. While absorption bands at 1384 and 1105 cm^{-1} could be ascribed to C-O bond from reduced graphene oxide. (Gao *et al.,* 2014; Aijiao *et al*., 2017).

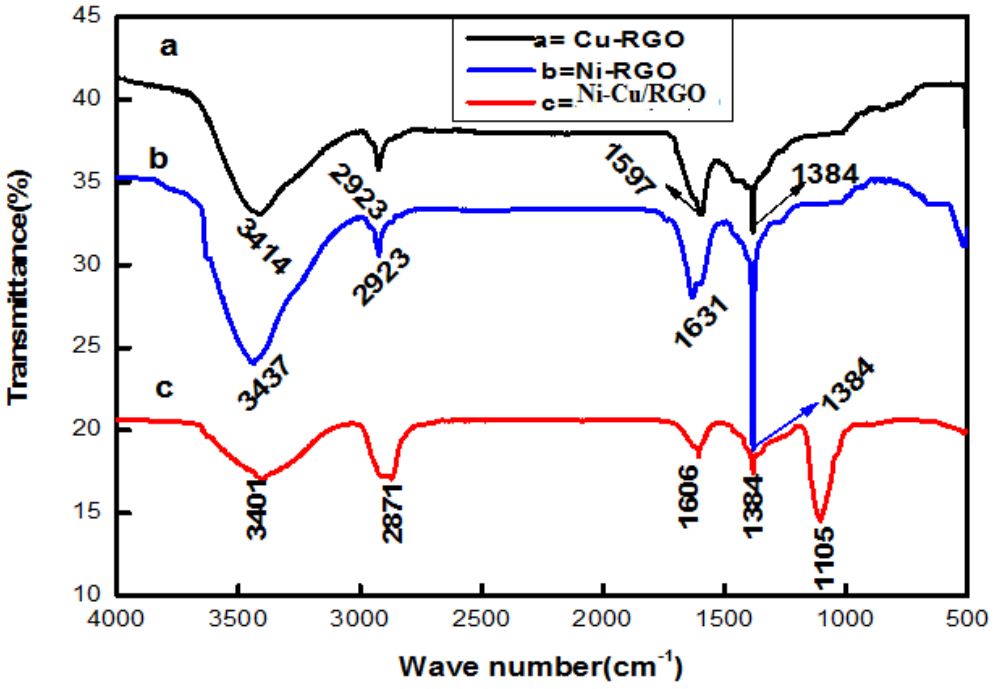

Figure 11. FTIR spectra of Cu-RGO, Ni-RGO and Ni-Cu/RGO nanocomposites

4.1.3. UV Analysis

The Uv-vis absorption spectrum Fig.12 of the synthesized Ni-Cu/RGO nanocomposites exhibits one broad band with a maximum at 530 nm. It can be assigned to the **Π-Π*** transition of C=C bonds of the carbonyl system (Zhong *et al*., 2010). The spectra show absorption edge

of the Cu-rGO, Ni-RGO at around 490 and 510 nm, showing these nanocomposites being blue shifted as compared to Ni-Cu/RGO for which the peak is at 530 nm. The band gap energy in a nanocomposite could be obtained from the absorption maxima, using the formula:

$$\mathbf{Eg = hc/\lambda_{max}\ (eV)} \qquad \mathbf{(4.1)}$$

Where h=Plank's constant and Eg = energy band gap (Kemary et al., 2010) .The calculated band-gap value of the nanocomposite for Ni-Cu/RGO was 2.34eV, which is red- shifted from the Cu-rGO, Ni-RGO, Eg = 2.54 and 2.44 eV, respectively. From the band gap, it can be observed that Ni-Cu/RGO composite has the lowest band gap energy value (2.34eV), the decrease in the band gap between the valence band and conduction band, hence, the excitation of electron from valence band to conduction band required lower energy and thus higher in conductivity (Yang *et al*, 2013).

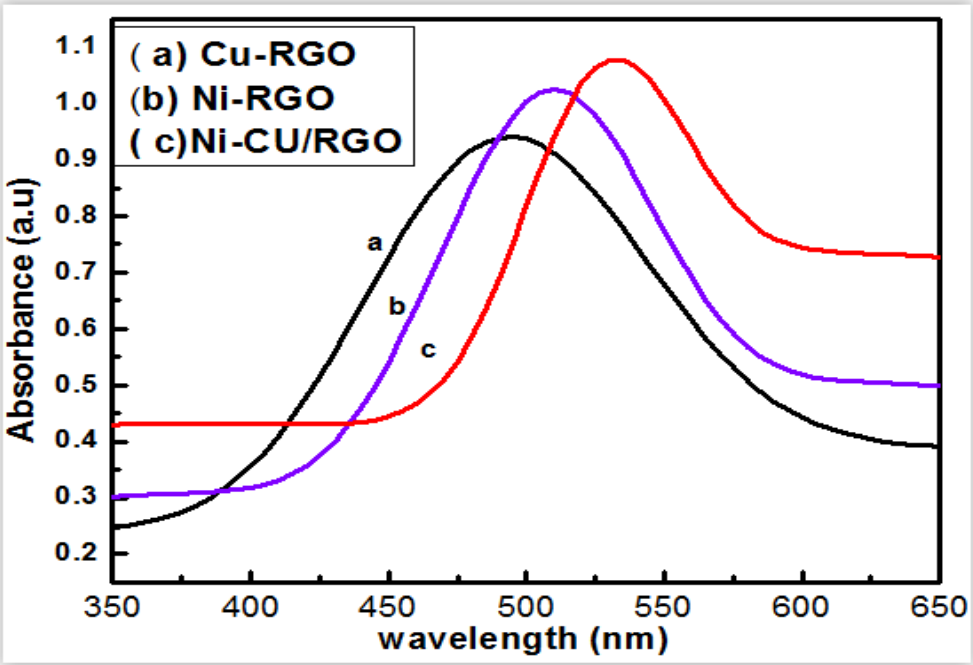

Figure 12. Uv-vis diffuse reflectance spectra

4.1.4. SEM and EDX Analysis

Fig.13 (a), (b) and (c) present the SEM images and EDX of Cu-RGO, Ni-RGO and Ni-Cu/RGO in 100 magnifications. Fig.13 (a) shows the SEM image of Cu-RGO nanocomposite, which has no distinct morphology, but there is aggregation of irregularly shaped nanoparticles of various sizes on RGO matrix. Moreover, the SEM micrograph of Cu-RGO composites associated with EDX is shown in Fig.13 (a). The presence of the required elements is confirmed from the EDX spectra. The weight ratio of the metal to nonmetal (RGO) demonstrates the presence of the Cu in pronounced proportion (Table 4). Fig. 13 (b) shows the SEM images of Ni-RGO nanocomposite, with bright spherical morphology of Ni nanoparticles deposited on the surface of predominantly amorphous RGO. The presence of Ni is confirmed from the EDX spectra and Table 4. Similarly in the case of Ni-Cu/RGO in Fig.13 (c), the bright smaller particles are observable for the metals. The metal nanocomposites are deposited on the surface of RGO in the same way. Moreover, to confirm the presence of Ni and Cu elements we have also carried out the EDX analysis.EDX spectra of Ni-Cu/RGO recorded from JSM-IT300 is shown in Fig. 13(c). As expected, copper, nickel, carbon and oxygen elements are detected. The carbon element comes from the RGO nanospheres, while oxygen mainly from the residual oxygen-containing functional groups on RGO. It was found that the content of Ni and Cu in the composites is 61.8 and 29.6 wt%, and the molar ratio of Ni/Cu is about 0.7:0.3, which is in agreement with the initial molar ratio of $Cu^{2+}$and Ni^{2+}ions.

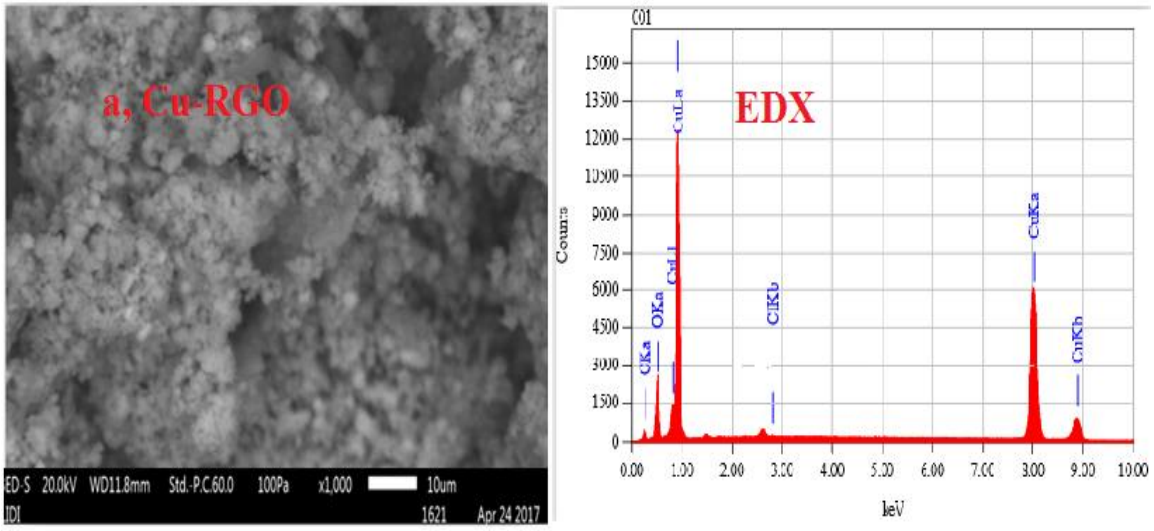

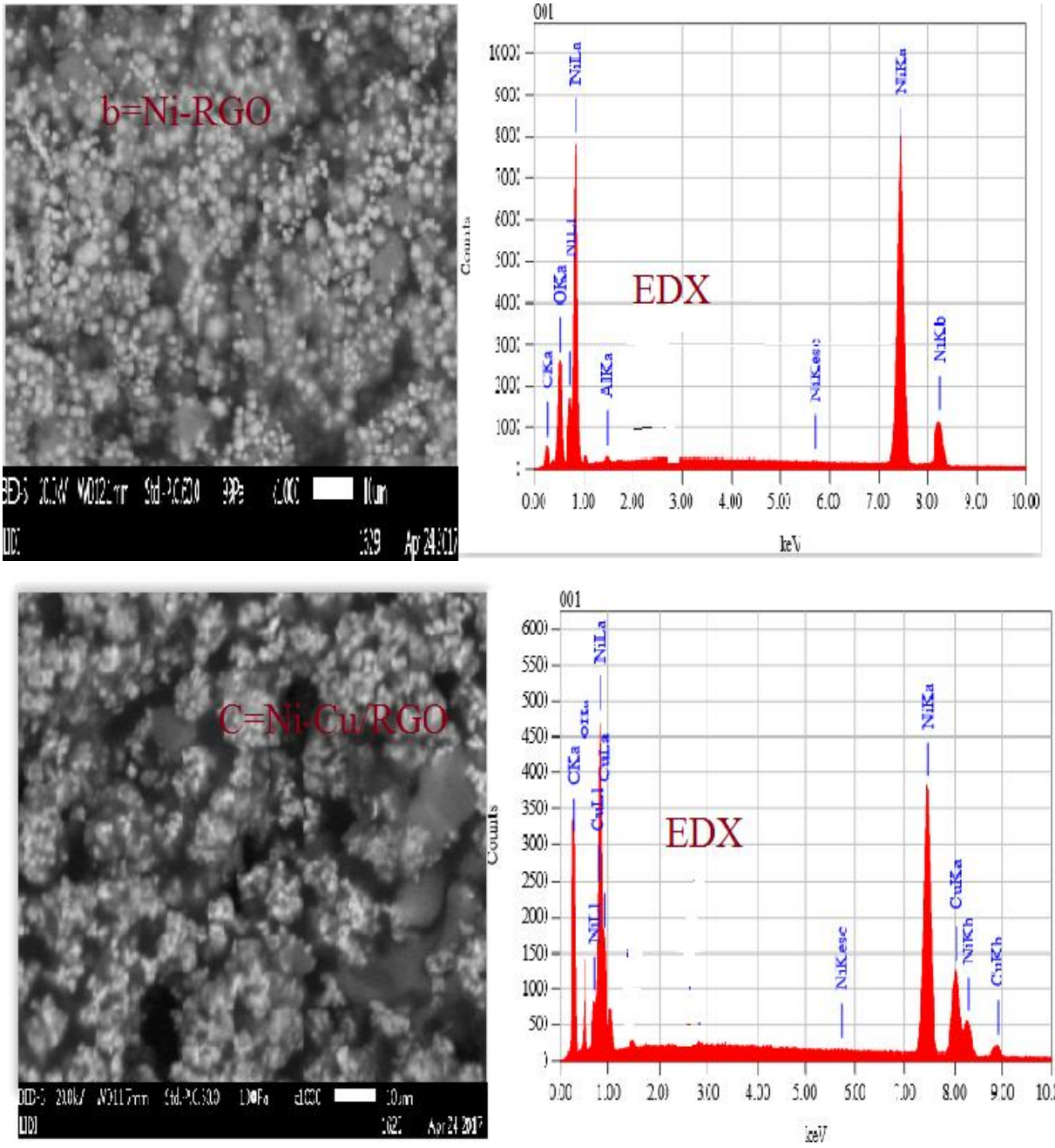

Figure 13. a, b and c, SEM images and EDX spectra of Cu-RGO, Ni-RGO an Ni-Cu/RGO

Table 4. The composition of nanocomposite analyzed by SEM (% in weight), EDX analysis

Nanocomposites	Element	Weight%	Atom%
Cu-RGO	Cu	93.55	69.17
	C	2.66	13.38
	O	3.09	16.61
	Cl	0.7	0.84
Total		100.0	100.0
Ni-RGO	Ni	93.96	67.35
	C	2.82	15.95
	O	2.92	16.26
	Al	0.3	0.44
Total		100.0	100.0
Ni-Cu/RGO	Cu	29.60	27.38
	Ni	61.8	63.06
	C	5.44	5.04
	O	3.16	4.52
Total		100.0	100.0

4.2. Electrochemical Properties of Ni-Cu/RGO Nanocomposite

4.2.1. Electrochemically Active Surface Area

Platinum electrode modified by Cu-RGO, Ni-RGO and Ni-Cu/RGO nanocomposite was studied in 0.1 M NaOH at scan rate of 50 mV/s by cycling the potential between -0.4 to 0.6 V. Potential. The voltammogram curves recorded are shown in Fig. 14(a). As can be seen oxidation peak appeared around -0.18 V and reduction peak occurred at -0.21V is due to the hydrogen adsorption/desorption processes in this potential region (Muhammad *et al.,* 2014). The cathodic peaks appear at about 480 mV may be related to the regeneration of Cu (II) and Ni (II) species (Ezhil *et al* 2016).

The electrocatalytic surface area (ECSA) of the electrocatalysts can be calculated from the Coulomb charge for hydrogen adsorption and desorption (QH) in the negative-going potential scan -0.4 to 0.6 V versus Ag/AgCl. The calculation of the (ECSA) can be made using Eq 4.1 (Andisiwe, 2013):

$$\mathbf{ECSA} = \frac{\mathbf{QH}}{\mathbf{208xWpt}} \qquad \mathbf{(4.2)}$$

where Pt represents the platinum-loading (g/cm^2) of the electrode, Q_H is the charge for hydrogen desorption (mC/cm^2). The ECSA is calculated by assuming a value of 208 mC/cm^2 for the adsorption of a hydrogen monolayer. Ni-Cu/RGO electrocatalysts exhibited a higher ECSA (89.1cm^2/g), than Ni-RGO (74.04 cm^2/g) and Cu-RGO (57.05 cm^2/g) most likely because of the high specific surface as a result the porous surface and small particle of the composite. This may significantly influence the electrocatalytic activity the material for methanol electro-oxidation as in the literature (Ezhil *et al* 2016).

4.2.2. Electrochemical Behaviors of the Ni-Cu/RGO in the Presence of $K_3Fe(CN)_6$

Figure 14(b) presents the cyclic voltammograms of 1 mM $K_3Fe(CN)_6$ in 0.1 M KCl on Cu-RGO, Ni-RGO and Ni-Cu/RGO nanocomposite modified electrodes at a scan rate of 50 mV/s. The electrochemical parameters are shown in Table1 in the Appendix and it was observed that Ni-Cu/RGO results a smaller peak potential separation (ΔEp = 61 mV) and larger peak current than those of a bare Pt electrode (ΔEp =69 mV, Cu-RGO ΔEp = 66 mV and Ni-RGO ΔEp = 64 mV indicating a rapid electron transfer and larger electroactive surface area for the nanocomposite. The clear increase in the anodic and cathodic peak current of the Ni-Cu/RGO nanocomposite compared to the binary systems indicates an increase in the electroactive surface area both from the contribution of the Cu and Ni nanoparticle. Particularly, the Ni-Cu/RGO nanocomposite modified electrode showed a ΔEp value around to the ideal kinetics (59 mV) of a one-electron reversible process, suggesting the excellent conductivity and ideal reversibility of the redox reaction (Ezhil *et al* 2016).

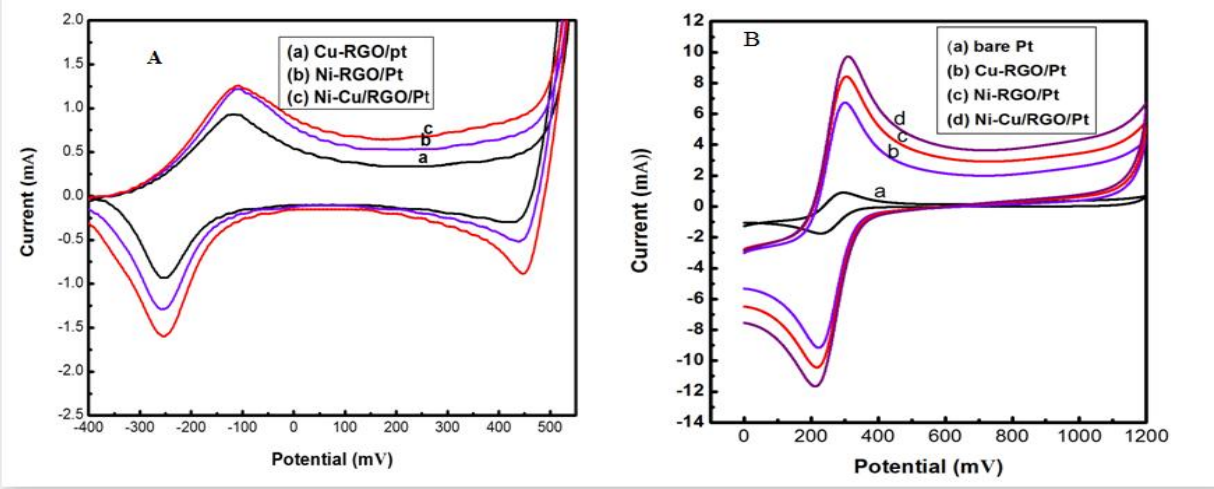

Figure 14 . (A) Cyclic voltammogram of (a) Cu-RGO, (b) Ni-RGO and (c) and Ni-Cu/RGO nanocomposite modified Pt electrodes in 0.1 M NaOH; (B) 1 mM $K_3[Fe(CN)_6]$ in 0.1 M KCl (a) bare Pt, (b) Cu-RGO, (c) Ni-RGO and (d) Ni-Cu/RGO nanocomposite modified electrodes at a scan rate of 50 mV/s

To understand further the electrochemical property of Ni-Cu/RGO nanostructure, the effect of scan rate on the modified electrode was conducted in the presence of 1mM K_3 Fe (CN) $_6$ in 0.1 KCl. As can be seen from the voltammograms in Fig.15 (A) the anodic and the cathodic peak current remains constant and the separation between peak to peak potential was in the range of 60-65 mV as the scan rate increases (Table 2 Appendix). This demonstrates oxidation and reduction process on Ni-Cu/RGO surface is reversible process and enhances fast electron transfer. Besides, the fact that plot of anodic peak current versus the square roots of scan rate is linear (Fig.15 B); the redox process of potassium ferricyanide on the surface of Ni-Cu/RGO modified electrode is a diffusion controlled process.

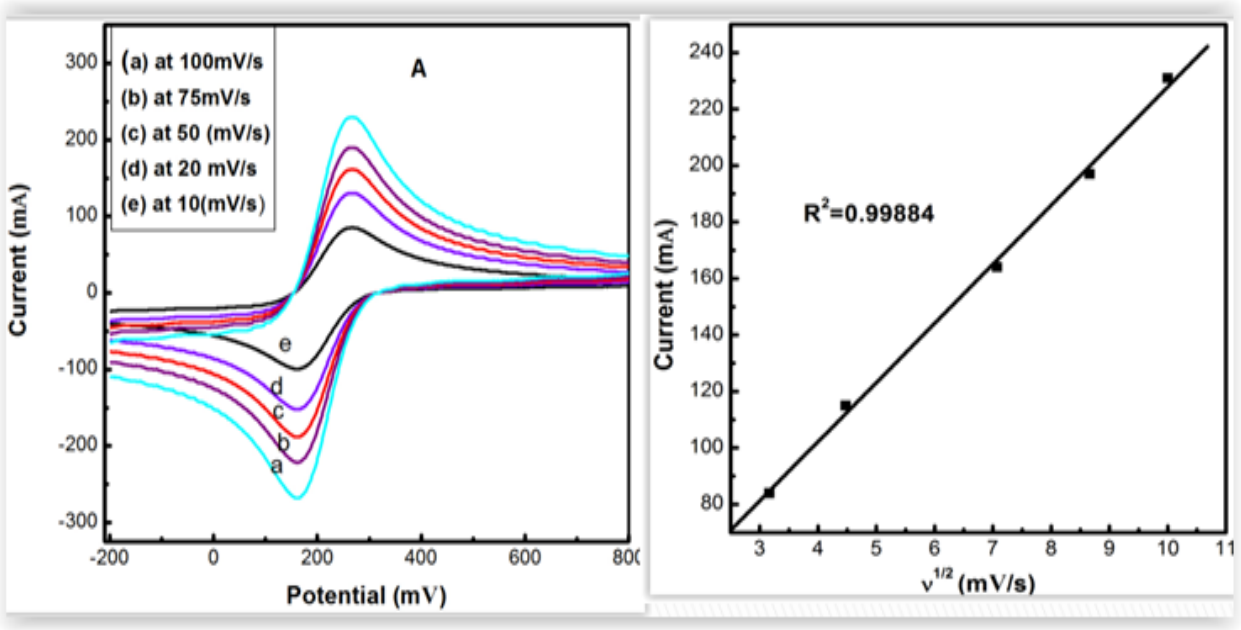

Figure 15. A) Scan rate dependence of 1 mM $K_3Fe(CN)_6$ in 0.1 M KCl (10 to 100 mV/s); B) plot of peak current vs Square roots of scan rate

4.2.3. Electrochemical Oxidation of Methanol at Ni-Cu/RGO Nanocomposite

The electrochemical activity of the as-prepared Cu-RGO, Ni-RGO and Ni-Cu/RGO electrocatalysts, and Pt bare electrocatalysts for methanol oxidation reaction was investigated by CV in 0.1M NaOH at scan rate of 50 mV/s in the presence of 0.1 M methanol. Nickel nanostructure plays a decisive role in the electrochemical oxidation of methanol and it is well studied and reported in the literature the mechanism of the electrocatalyst is indicated in Equation (1-6).

$Ni + 2OH^- \longrightarrow Ni(OH)_2$ 1

$CH_3OH + Ni(OH)_2 \longrightarrow Ni(OH)_2(CH_3OH)ad$ 2

$Ni(OH)_2 + OH^- \longleftrightarrow NiOOH + H_2O + e^-$ 3

$Ni(OH)_2(CH_3OH) + OH^- \longrightarrow NiOOH(CH_3OH)\ ads\ H_2O + e^-$ 4

$NiOOH(CH_3OH) + NiOOH + OH^- \longrightarrow Ni(OH)_2 + NiOOH(COH)\ ads + H_2O + e^-$ 5

$NiOOH(COH)\ ads + OH^- \longrightarrow Ni(OH)_2 + HCOO^-$ 6

The results in this study and together to literature reports (Jafarian *et al.,* 2006) supported the reaction path way for methanol oxidation. For example, as can be read from the cyclic voltammogram Fig. 16, the anodic peak occurred around 0.4 V is due to methanol oxidation whereas the small peak around 0.33V is most probably is due to oxidation of Ni (II) to regenerate Ni (III) whereas the peak formed during the cathodic scan is the reduction of Ni(III) to Ni(II). Since Cu is thermodynamically stable in the region where Ni acts as a catalyst, its role is to fill the vacant d-band of Ni so that it reduces the possible strong adsorption of reactants and products on the surface of Ni-Cu/RGO (Jafarian *et al*., 2006). The effect of scan rate on the performance of Ni-Cu/RGO electrocatalyst for methanol oxidation in alkali medium is displayed in Fig.16 (A). As the scan rate increases, there is a slight shift in the oxidation peak potential toward more positive values and the peak currents (i_p) increase linearly with the square root of the scan rate Fig.16 (B). These observations illustrate electrochemical oxidation of methanol is a diffusion-controlled process. Similar finding has been reported by Wang *et al.,* (2006) by oxidizing methanol using RGO/CoO_4 nanocomposite The diffusion coefficient methanol calculated using , the Randles-Sevcik equation can be written in a more concise form,

$$\mathbf{i_p = (2.69)x10^5 n^{3/2} V^{1/2} D^{1/2} A C} \qquad \mathbf{4.3}$$

where A is electrode surface area(cm^2), *D* is the diffusion coefficient (cm^2/s), *C* is the concentration of the electroactive species in the bulk solution (mol/cm^3) and ν is the scan rate (V). Therefore, i_p is proportional to *C* and proportional to $V^{1/2}$, the D value was found to be $2.6x10^{-4}cm^2/s$, our data agree well with the values reported by Jafarian *et al*., (2006), $2.16\ x10^{-4}cm^2/s$

The electron transfer coefficient, α_s and electron transfer rate constant ,k_s could be determined based on Laviron Equation

$$\mathbf{Epa = E^o + \frac{RT}{(1-\propto)nF} - \frac{RT}{(1-\propto)nF} lnv} \qquad \mathbf{4.4}$$

$$\mathbf{Epc = E^o + \frac{RT}{\propto nF} - \frac{RT}{\propto nF} lnv} \qquad \mathbf{4.5}$$

$$\ln K_s = \alpha\ln(1-\alpha) + (1-\alpha)\ln\alpha - \ln\left(\frac{RT}{nFv}\right) - \alpha(1-\alpha)\left(\frac{nF\Delta E}{RT}\right) \qquad 4.6$$

α Can be calculated from the slope of Ep *vs* lnv

$$\text{Slope} = \frac{RT}{(1-\alpha)nF} \qquad 4.7$$

The α value was calculated as 0.91 and K_s= 2.38 s^{-1}. This indicates super kinetic. Our data agree well with the values reported by Ciszewski *et al*., 2003), 1.979 s^{-1} .

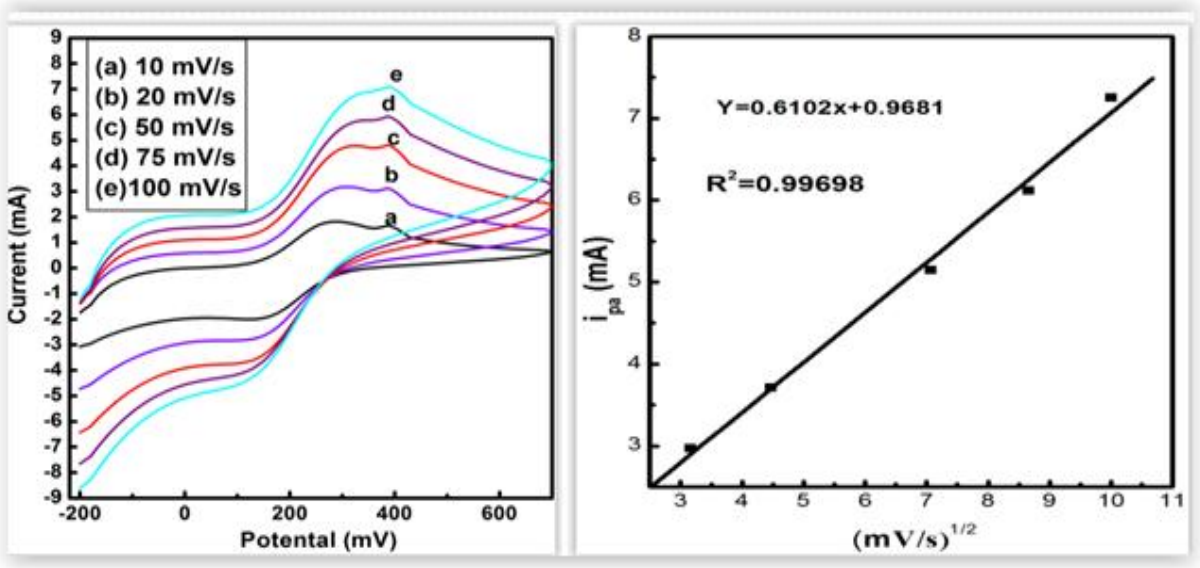

Figure 16 . (A) Cyclic voltammograms recorded during electrochemical oxidation of 0.1 M methanol on Ni-Cu /RGO electrocatalyst in 0. 1 M NaOH at scan rates of a) 10, b) 20, c) 50, d) 75 and e) 100 mV/s. (B) The relationship between the peak currents and the square roots of the scan rate

For comparison purposes, cyclic voltammograms oxidation of methanol was also recorded on bare Pt, Cu-RGO, Ni-RGO and Ni-Cu/RGO nanocomposites modified electrodes under the same conditions (Fig.17) Ni-Cu/RGO nanocomposite modified electrode shows a higher electrocatalytic oxidation current density during forward (440 mA) compared to the other modified electrodes (Cu- RGO, and Ni-RGO, 242 and 353 mA, respectively). This is most likely to the synergic effect of Ni and RGO which results high porous, electro catalytic, large surface area and high conductive of Ni-Cu/RGO. This behavior of the ternary system is

supported from the results obtained from XRD, SEM, FTIR and Uv-vis experiments (Tripkovic *et al.*, 2004).

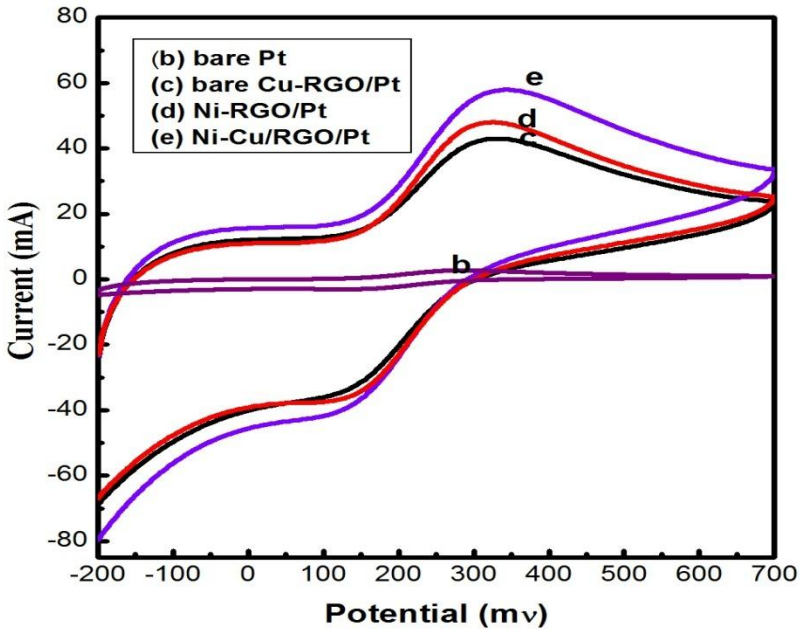

Figure 17. Cyclic voltammograms recorded during electrochemical oxidation of 0.1 M methanol on bare Pt and Cu-RGO, Ni-RGO and Ni-Cu/RGO-modified electrodes in solution of 0.1M NaOH at a scan rate of 50 mV/s

4.2.4. Influence of Methanol Concentration on the Electrocatalytic Activity of Ni-Cu/RGO

The concentration of methanol is an important factor to be considered in the practical application of methanol fuel cells. The CV and linear sweep voltammetry (LSV) were used to investigate the influence of the methanol concentration (0.1 M to 2.0 M) in 0.1 M NaOH on the performance of Ni-Cu/RGO nanocomposite modified electrode at a scan rate of 50 mV/s and the results are displayed in Fig. 18. As the methanol concentration increased in the electrolyte solution results in an initial increase in the peak response up to a methanol concentration of 1.5 M followed by a decreasing response with a further increase in methanol concentration. The most probable reason for this appears to be a poisoning of the electrode due

to accumulation of methanol oxidation products on the surface, and we assume this effect caused by saturation of active sites of the surface electrode (Tripkovic *et al.*, 2004).

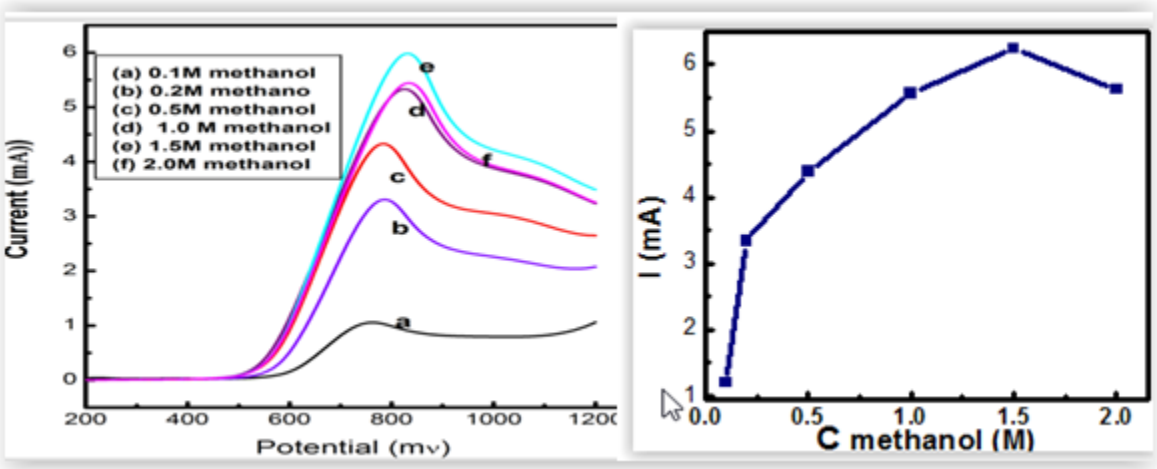

Figure 18. LCV of methanol oxidation at different concentrations (0.1 to 2.0 M) + 0.1 M NaOH on Ni-Cu/RGO/Pt electrode at 50 mV/s.

4.2.5. Reversibility and Stability of Ni-Cu/RGO Modified Electrode for Methanol Oxidation

Stability and reversibility are also important parameters that have to be considered for an electrocatalyst for any possible potential practical applications. Ni-Cu/RGO ternary system was considered since it is more sensitive to methanol oxidation in comparison to the binary systems as confirmed from CV and LSV results. The stability of Ni-Cu/RGO was tested using 0.1 M methanol in 0.1 M NaOH by cycling the potential in between -0.1V to 0.6V at scan rate of 50 mV/s. A total of 80 cycles was recorded and the first three, 40^{th}, 39^{th}, 38^{th}, and the last two cycles the voltammogram is shown in (Fig.19). The peak current decreased gradually with further expansion of the cycle number and the electrocatalyst could not give response after 80 cycles because it was observed that Ni-Cu/RGO not stayed longer on the surface of electrode as it was not attached well by appropriate binder.

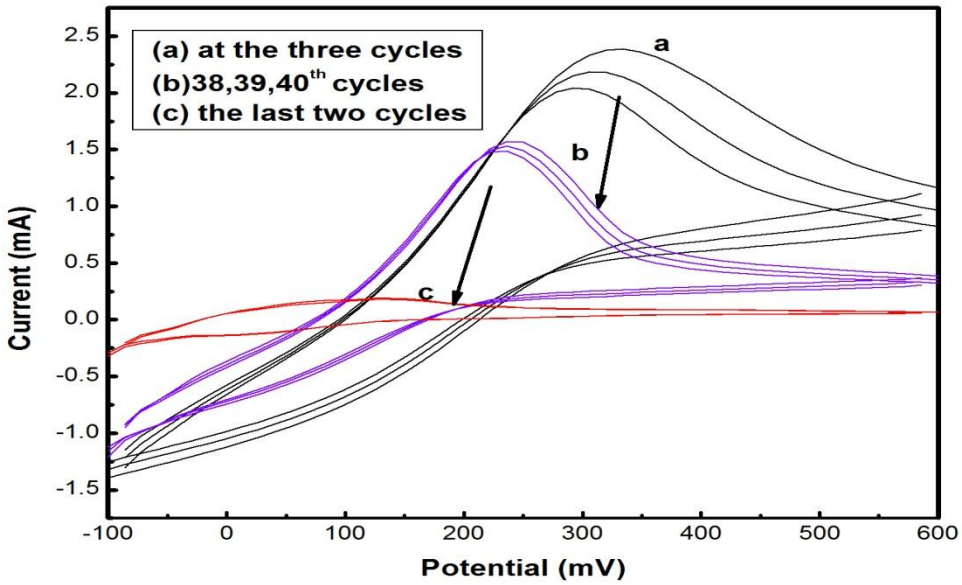

Figure 19. CVs of 0.1 M methanol/0.1 M NaOH a scan rate of 50 mV/s on the surface of Ni-Cu/RGO modified Pt electrodes a) the first three cycles b) 40, 39 and 38 cycles and c) the last two cycles

4.2.6. Chronoamperometry

Chronoamperometry experiments was done using 0.1 M methanol in 0.1M NaOH aqueous solution by applying a constant potential of 0.47 V for 300 s to assess the stability Ni-Cu/RGO electrocatalyst and to compare further its performance with the bare Pt and to that of the binary systems Cu-RGO, Ni-RGO, and Ni-Cu -RGO. It can be observed from Fig. 20 that there was an initial rapid decrease in the decay current density for all cases due to the formation of reactive intermediates, such as COHads and COOHads during the methanol oxidation (Ezhil *et al*., 2016). After the duration of 150s, the current reached a constant for Cu-RGO, Ni-RGO, and Ni-Cu/RGO 11, 11 and 45 mA, respectively. It was noticed that the current for the bimetallic and reduced graphene oxide composite about four times higher than that of the Cu-RGO as well as Ni -RGO catalyst. As long as 200 s, the current remained at 43 mA for the ternary system indicating its better stability over that of the Cu and Ni alone. This demonstrates the better tolerance of Ni-Cu/RGO to the intermediate species for methanol

oxidation. A similar report is available in the literature for the oxidation of methanol for example over Pt-Au/RGO nanocomposite (Ezhil *et al.*, 2016*).*

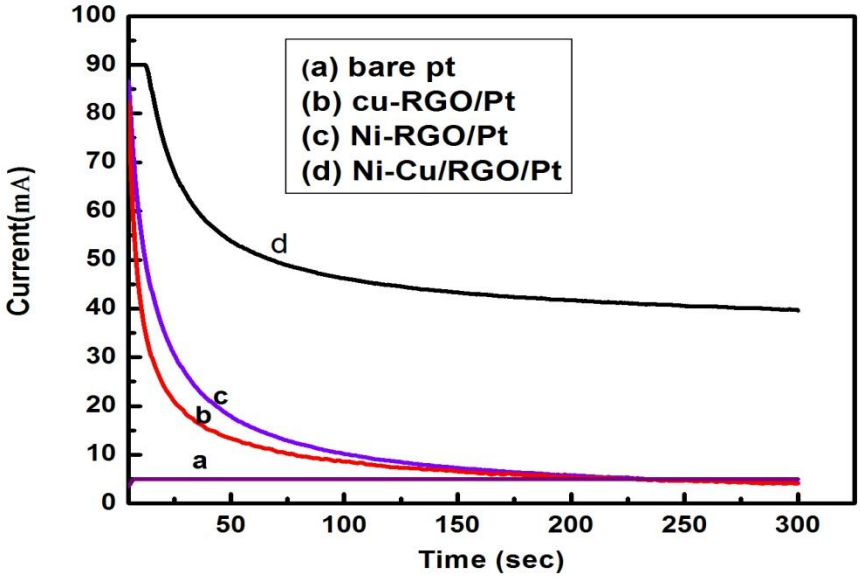

Figure 20. Chronoamperometry curves showing methanol oxidation

4.2.7. Electrochemical Impedance Spectroscopic Studies

To investigate the electrocatalytic performance of the as synthesized nanocomposites, electrochemical impedance spectroscopic (EIS) analyses were performed in the frequency range from 0.1 Hz to 1000 Hz by applying a DC offset potential of 0.47 V and a voltage of AC amplitude 5 mV in a solution of 0.1 M methanol in 0.1 M NaOH. The Nyquist plot for Cu-RGO, Ni-RGO and Ni-Cu/RGO is shown in Fig. 21. A semicircle is observed in most of the frequency region. As seen from the Nyquist plot, the diameter of the semicircle for Ni-Cu/RGO is smaller indicating lower charge transfer resistant in comparison with the others nanocomposites Ni-RGO and Cu-RGO, respectively. This demonstrates the synergic effect of Ni nanoparticle and RGO which results in high surface area and catalytic properties of Ni-Cu/RGO. So that ternary system facilitates electro-oxidation kinetics of methanol and EIS

result (6,761, 6,574 and 5,249 Ω corresponding to Cu-RGO, Ni-RGO and Ni-Cu/RGO, respectively) which is in line with that of data recorded from CV and chronoamperometry analysis (Wang *et al.*, 2006).

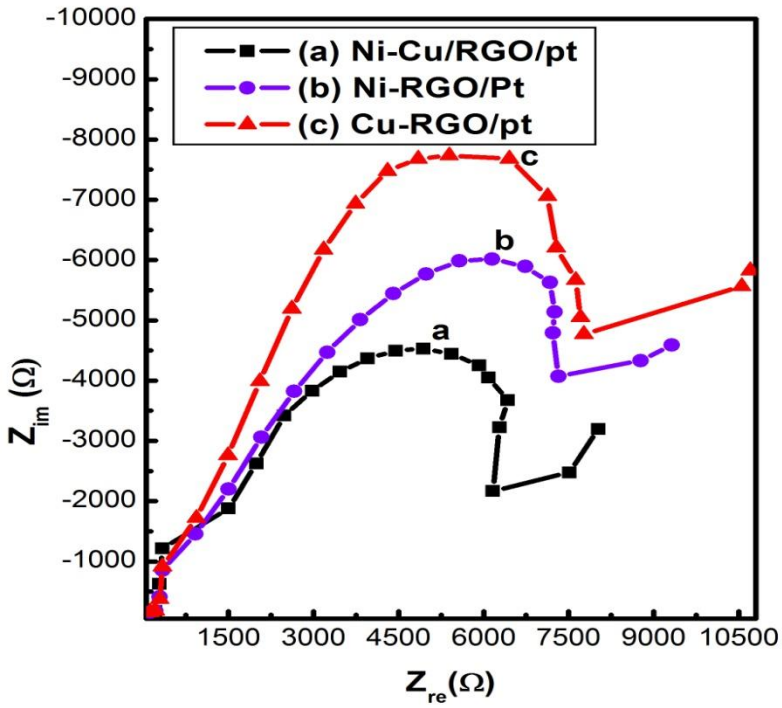

Figure 21. Nyquist plots for EIS study of 0.1M methanol/0.1M NaOH on the electrocatalysts a) Ni-Cu/RGO, b) Ni-RGO, and c) Cu-RGO modified electrode at a DC potential of 0.45V and amplitude 5 mV

Figure 22 shows the Bode-phase plots of various modified electrodes in the frequency range of 0.1–1000 Hz. Higher phase peak intensity can be seen at a frequency range of 300–500 Hz, which is attributed to the charge-transfer resistance of the modified electrode. Interestingly, the phase peaks in the Bode plots for the Cu-RGO, Ni-RGO and Ni-Cu/RGO nanocomposite modified electrode are shifted to a low frequency region of 0.1–100 Hz as a result of the high electron transfer behaviour of the modified electrodes

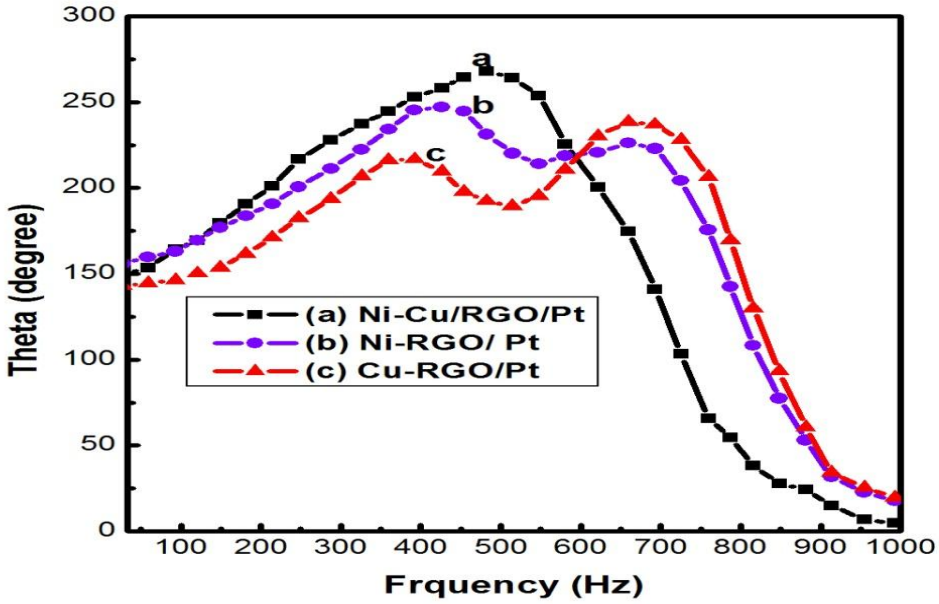

Figure 22. Bode Plot for EIS study of 0.1M methanol/ 0.1M NaOH on the electrocatalysts a) Ni-Cu/RGO, b) Ni-RGO, and c) Cu-RGO modified electrode at a DC potential of 0.45V and AC amplitude 5 mV

5. SUMMARY, CONCLUSION AND RECOMMENDATION

5.1. Summary

Ni-Cu/RGO, Ni-RGO and Cu-RGO have been successfully synthesized using chemical reduction method and used as catalysts for electro-chemical oxidation of methanol in alkaline medium. The as synthesized nanostructured materials were characterized by employing uv-visible, FTIR, XRD, EDX and SEM. The result obtained from XRD patterns testified the Ni-Cu/RGO nanoparticles with a cubic crystalline state on the surface of RGO and with a smaller particle size about (6.83 nm) and that of Ni-RGO (8.86 nm) and Cu-RGO (11.94) nm. SEM topographical image of Ni-Cu/RGO is spherical morphology.

Electrochemical behaviors of Ni-Cu/RGO, Ni-RGO and Cu-RGO were investigated using CV, LSV, CA and EIS techniques. Methanol electro- oxidation was enhanced on the surface of Ni-Cu/RGO modified platinum electrode when compared with the other electrocatalysts. This is most probably due to the porous nature of the material, catalytic property of Ni and RGO and the high electrical conductivity enhance electron transfer on the electrode interface. 80 potential cycles recorded in the range of -0.1 to 0.7 V indicated the stability of the electrocatalyst since degradation of the peak current is minimal in the subsequent cycles in consistent with that of the chronoamperometry experiment. EIS study also demonstrated, high electron transfer kinetics since the semicircle appeared in most of the frequency range is small relative to that of the binary systems. Therefore, the performance of Ni-Cu/RGO for methanol electro-oxidation was much better than the others and the results recorded from the different techniques employed in this study in agreement and support the claims.

5.2. Conclusion and Recommendations

XRD and SEM revealed that all the synthesized electrocatalysts possessed spherical structure, and small particle size in agreement to the literature values. All electrochemical data indicated Ni-Cu/RGO modified Pt electrode was a suitable material for the electro-oxidation of methanol in NaOH solution. This new electrode material may have a potential application for efficient electrochemical oxidation of methanol in fuel cells.

In this study the poor stability of the nanocomposites at vey larger potential cycles is due the absence of appropriate binding agent that keeps the material longer on the electrode surface. Hence studying the electrochemical behaviours of the as synthesized nanocomposites in the presence of a binder is recommended. Besides, optimization to find the appropriate composition for Ni-Cu/RGO nanocomposite is also important and it should be considered for future study.

6. REFERENCES

Abdel, MA., Abdel, RM. and Khalil, MW.2004 .Nickel as a catalyst for the electro-oxidation of methanol in alkaline medium. *Journal of Power Sources*, 134: 160-169.

Alegre, C., Calvillo, L., Moliner, R., González-Expósito, J.A., Guillén-Villafuerte, O., Martinez Huerta, M.V., Pastor, E. and Lázaro, M.J.2011. Pt and PtRu electro catalysts supported on carbon xerogels for direct methanol fuel cells. *Journal of Power Sources*, 196: 4226–4235.

Alexandre Hacquard. 2005. Improving and Understanding Direct Methanol Fuel Cell (DMFC) Performance a Thesis submitted to the faculty of Worcester Polytechnic Institute.

Andisiwe, B. 2013. Electrochemical study of electrode support material for direct methanol fuel cell applications. Doctorial Dissertation, University of the Western Cape, South Africa.

Ankur, P. and Manivannan, R.2015. A Study on Synthesis of Nickel Nanoparticles Using Chemical Reduction Technique. *Journal of Recent Patents on Non medicine,* 5:1-5.

Antolini, E., Salgado, J. R. and Gonzalez, E. R.2006. The methanol oxidation reaction on platinum alloys with the first row transition metals: The case of Pt–Co and –Ni alloy electro catalysts for DMFCs. *Applied Catalysis B: Environmental*, 63: 137–149.

Arico, A.S., Baglio, V., Modica, E., Di Blasi, A., Antonucci V. 2004. Performance of DMFC anodes with ultralow Pt loading, *Electrochemical Communication*, 6:164-169.

Arulmary, A., Manivannan, L., John Kennedy, M., Bououdina. Sundaram J., Judith, V.2014. Structure and magnetic properties of Cu−Ni alloy nanoparticles prepared by rapid microwave combustion method. *Journal of Transition Nonferrous Metal*, 24: 1467−1473.

Asanda, N. 2010. Electrochemical Investigation of Platinum Nanoparticles Supported on Carbon Nanotubes as Cathode Electro catalysts for Direct Methanol Fuel Cell. MSc Thesis, University of the Western Cape.

Balgis, R., Anilkumar, G.M., Sago,S., Ogi ,T. and Okuyama.K , K.2012. Nanostructured design of electrocatalyst support material for high-performance PEM fuel cell application. *Journal of Power Sources,* 203: 26-33.

Baomin, L., Shan, X., Xingbin, Y. and Qunji, X.2012.Synthesis and electrochemical properties of graphene supported PtNi nanodendrites. *Electrochemistry Communicatio-ns*, 23: 72–75.

Bard Allen, J. and Faulkner Larry,R.2001.Electrochemical methods Fundamentals and applications Second edition. Department of Chemistry and Biochemistry University of Texas at, Austin.

Bong, S., Kim, Y.R., Kim, I., Woo, S., Uhm, S., Lee, J.and Kim, H. 2010.Graphene support electro catalysts for methanol oxidation. *Journal of Electrochemical Communication*, 12: 129–131.

Calvillo, L., zaro, M. J., Suelves, I., Echegoyen, Y., Bordej, G.and Moliner, R. 2009. Study of the Surface Chemistry of Modified Carbon Nanofibers by Oxidation Treatments in Liquid Phase. *Journal of Nanoscience and Nanotechnology*, 9: 4164-4169.

Castro, E.G., Salvatierra, R.V., Oliveira, M.M, Schreiner,W., Zarbin,A.G. 2009. International conference on Advance Materials.

Celorrio, V., Montes , M.G., Plana, D., Moliner, R., Fermín, D.J. and Lázaro, M.J.2012.Electr ochemical performance of Pd and Au–Pd core–shell nanoparticles on surface tailored carbon black as catalyst support. *International Journal Hydrogen Energy* ,37: 7152-7160.

Cheng, L.Q., Shen, P.K. and Liu, Y.L.2007. Methanol and ethanol electro-oxidation on Pt and Pd supported on carbon microspheres in alkaline media. *Electrochemistry Communication*, 9: 997–1001.

Chia-Liang Sun, Jheng-Sin, Jui-Hsiang Tang, Meng-Chi Lin, Jhing-Jhou Wua, Nen-Wen Pu, Gia-Nan Shi, Ming-Der Ger.2014. Investigation of the adsorption of size-selected Pt colloidal nanoparticles on high-surface-area graphene powders for methanol oxidation reaction. *Journal of the Taiwan Institute of Chemical Engineers*, 45:1025–1030.

Christophe, M., Doneux, T and Buess-Herman,C.2012. Electroreduction of Carbon Dioxide on Copper-Based Electrodes: Activity of Copper Single Crystals and Copper-Gold Alloys. *Journal of Electrocatalysis*, 3: 139–146.

Danafar, F., Fakhrúl-Razi, A., Salleh, M. and Biak, A .2009. Fluidized bed catalytic chemical vapour deposition synthesis of carbon nanotubes. *Journal of Chemical Engineering*, 155: 37- 48.

Dreyer, D.R., Park, S., Bielawski.C.W and Ruoff .R.S.2010. The chemistry of graphene oxide. *Journal of Chemical Society*, 39(1): 228–240.

Dubau L., Countanceau C., Garnier E., Leger, J. M. and Lamy, C. 2003 .Electro-oxidation of methanol at platinum–ruthenium catalysts prepared from colloidal precursors: Atomic composition and temperature effects. *Journal of Applied Electrochemistry*, 33: 419–429.

Eda, G., Fanchini, G. and Chhowalla, M.2008. Large-area ultrathin films of reduced graphene oxide as a transparent and flexible electronic material. *Journal of Natural Nanoparticle*, 3(5): 270–274.

Ezhil, A., Seung , K, Cheol, H. , Seo ,Y. , Chang, Y, Go-woon ,L., Jin Bae, L., Yun Suk, H. and Young-Kyu, H.2016. Pt-Au bimetallic nanoparticles decorated on reduced graphene oxide as excellent electro catalysts for methanol oxidation. *Journal of Synthetic Metals*, 219: 52–59.

Ferdowsi, G., Seyedsadjadi, S. and Ghaffarinejad, A.2015. Ni nanoparticle modified graphite electrode for methanol electrocatalytic oxidation in alkaline media. *Journal of Nanostructure Chemistry*, 5: 17–23.

Gao, H., Xiao, F., Ching, C. and Duan, H. 2011. One-step electrochemical synthesis of PtNi nanoparticle-graphene nanocomposite for non enzymatic amperometric glucose detection. *Journal of Applied Materials and Interfaces*, 8: 3049– 3057.

Gao, X., Jang, J. and Nagase, S.2009. Hydrazine and Thermal Reduction of Graphene Oxide: Reaction Mechanisms, Product Structures, and Reaction Design. *Journal of Physical Chemistry*, 114(2): 832–842.

Gyenge, E.2008. Chapter 4: Electrocatalytic oxidation of methanol, ethanol and formic acid', in PEM Fuel Cell Electro catalysts and Catalyst Layers, editor; Jiujun Zhang, Springer, New York, 165-270.

Hercules, M. and Ng, T.1976. Studies of nickel-tungsten alumina catalysts by X-ray photoelectron spectroscopy. *The Journal of Physical Chemistry*, 80(19): 2094–2102.

Isidorsson, J., Strømme, M., Gahlin, R., Niklasson, GA., Granqvist, CG. 1996. Ion transport in porous Sn oxide films: cyclic voltammogram interpreted in terms of a fractal dimension. *Solid State Communication*, 99: 109–111.

Jordan, M. and Anderson.2012. Electrochemical studies of nanoscale composite materials as electrodes in pemfuel cells. A dissertation of Doctor of Philosophy, University of Central Florida Orlando, Florida.

Jurzinsky, T., Cremers, C., Pinkwart, K. and Tübke, J. 2016. On the influence of Ag on Pd-based electro catalyst for methanol oxidation in alkaline media: A comparative differential electrochemical mass spectrometry study. *Journal of Electrochemical Acta*, 199: 70–279.

Jafarian , M.,Moghaddam,R., Mahjani,M. and Gobal,F.2006.Electrocatalytic oxidation of methanol on a Ni–Cu alloy in alkaline medium. *Journal of Applied Electrochemistry*, 36: 913–918.

Kamarudin, S.K., Achmad, F. and Daud, W.R.W.2009. Overview on the application of direct methanol fuel cell (DMFC) for portable electronic devices. *International Journal of Hydrogen. Energy*, 34(12): 6902–6916.

Kemary, El., Shamy, H. and Mehasseb,I .2010. Photo catalytic degradation of Ciprofloxacin drug in water using ZnO nanoparticles. *Journal of Luminescence*, 130: 2327–2331.

Lei,Y., Su, L.A., Jia, W.Z., Zhang, L.C., Beacham, C., Zhang, H., 2010. Facile Synthesis of a Platinum Nanoflower Monolayer on a Single-Walled Carbon Nanotubes Membrane and its Application in Glucose Detection. *Journal of Physical Chemistry*, 114(42): 18121-18125.

Leticia Garcia-Cruz, Alfonso Suez, Conch, O., Ania, José Solla-Gullón, Thies Thiemann, Jesus Iniesta and Vicente Montiel1.2014. Electrocatalytic activity of Ni-doped

nonporous carbons in the electro-oxidation of propargyl alcohol. *Journal of Applied Chemistry*, 73: 1-26.

Liquan Lu1, Shichao Zhan and Shaohui Yan, 2015. Electro-oxidation of methanol on AuNi/C Catalyst in Alkaline Medium. *International Journal of Electrochemical Science*, 10: 649 – 658.

Liu,H., Song,C., Zhang,L., Zhang,J., Wang,H. and Wilkinson, D..2006. A review of anode cataly sis in the direct methanol fuel cell. *Journal of Power Sources*, 155: 95- 110.

Maiyalagan, T.2009. Pt–Ru nanoparticles supported PAMAM Dendrimer functionalized carbon nanofibers composite catalysts and their application to methanol oxidation. *Journal of Solid State Electrochemistry,* 13: 15-61.

Moganavally, P., Suresh, R., Deepa, M. 2014. Synthesis and characterization of bimetallic CuNi nanoparticles. *Journal of Applied Chemistry*, 7: 34-36.

Nilendri, R.2014. Synthesis, characterization, and catalytic activity of monometallic Pd and AgPd bimetallic nanoparticles in different solvent media. Dissertation National Institute of Technology, Rourkela.

Nordlund, J., Roessler, A .and Lindbergh, G. 2002.The influence of electrode morphology on the performance of a DMFC anode. *Journal of Applied Electrochemistry,* 32 (3): 259-265.

Ocampo, Miranda Hernandez, M., Morgado, J.,Montaya, J. and Sebastian ,P.2006. Characteriz ation and evaluation of Pt-Ru catalyst supported on multi-walled carbon nanotubes by electrochemical impedance. *Journal of Power Sources*. 160: 915-924.

Olson, E.J. and Buhlmann, P.2010.Minimizing hazardous waste in the undergraduate analytical laboratory: a microcell for electrochemistry. *Journal of Chemistry Education*, 87(11): 1260–126.

Ozkan, C.S., Paul, R.K., Ghazinejad, M., Penchev, M., Lin, J.A.and Ozkan, M., 2010. Synthesis of a Pillared Graphene Nanostructure: A counterpart of three-dimensional carbon architectures. *Journal of Architecture* 6(20): 2309-2313.

Park, S.J., Jung, H.J, Nah, C.W. 2003. Adsorption Properties of Fuel-Cell Electrode Produced from Activated Carbon Fibers in Three Phase Distribution, *Journal of Polymer*, 27: 46-51.

Pivovar, B.2014. Extended, Continuous Pt Nanostructures in Thick Dispersed Electrodes. In, Department of Energy Editor, USA.

Qiu, J. D., Wang,G. and Liang, R. P.2011. Controllable deposition of platinum nanoparticles on graphene as an electro catalyst for direct methanol fuel cells. *Journal of Physical Chemistry,* 115: 15639–15645.

Rahul, K., Diana, M., Fernandes, J., Cristina. F. and Elby, T.2016. Novel synthesis of highly catalytic active Ni-Cu/RGO nanocomposite for efficient hydrogenation of 4-nitrophenol organic pollutant. *International Journal of Hydrogen Energy* 4 1: 11608 -11615.

Roustom , B.E., Sine, G., Foci, G.and Comninellis, C.2007. A novel method for the preparation of bimetallic (Pt–Au) nanoparticles on boron doped diamond (BDD) substrate: application to the oxygen reduction reaction. *Journal of Applied Electrochemistry*, 37: 1227–1236.

Ruimin, D., Jinping, L., Jian, J., Fei, W., Jianhui, Z. and Xintang, H.2011. Tailored Ni–Cu alloy hierarchical porous nanowires as a potential efficient catalyst for DMFCs. *Journal of Catalysis Science and Technology*, 1:1406 –1411.

Schedin, F., Geim, S., Morozov, V., Hill, E., Blake, P., Katsnelson, M., and Novoselov, K .2007. Detection of individual gas molecules adsorbed on graphene. *Journal of Natural Material*, 6(9): 652–655.

Schumacher, S.,Andersson,K., Grabow,L., Mavrikakis,M., Nerlov,J. and Chorkendorff,I.2008. Interaction of Carbon Dioxide with Cu Over layers on Pt(111). *Journal of Surface Science*, 602: 702–711.

Sgro, L.2001.UV-visible spectroscopy of organic carbon particulate sampled from ethylene/air flames. *Journal of Chemosphere*, 42 (5-7): 671-680.

Siyavash, K., Mahsa, F., Minoo, D.and Ayoob, B.2013. Gold nanoparticles decorated reduced graphene oxide sheets with significantly high catalytic activity for ullmann homocoupling. *The Journal of Royal Society of Chemistry,* 4: 5243-5247.

Steigerwalt, S., Deluga, A., Cliffel, E. and Lukehart, C. M. 2001. A Pt−Ru/Graphitic Carbon nanofiber nanocomposite exhibiting high relative performance as a direct-methanol fuel cell anode catalyst. *Journal of Physical Chemistry*, 105: 8097–8101.

Subramanian,D., Balaji,G., Kumar,S. and Spivey,J.2009. Development of cobalt–copper nanoparticles as catalysts for higher alcohol synthesis from syngas. *Journal of Catalysis Today*, 147: 100–106.

Takasu, Y., Fujiwara ,T., Murakami, Y., Sasaki, K., Oguri ,M., Asaki ,T. and Sugimoto ,W., 2000. Effect of structure of carbon-supported PtRu electrocatalysts on the electrochemical oxidation of methanol. *Journal of Electrochemical Society*, 147: 4421-4427.

Tang, X., Zhang, B., Li,Y., Xu,Y., Xin,Q. and Shen,W. 2004. Structural features and catalytic properties of Pt/CeO_2 catalyst prepared by the modified reduction-deposition techniques. *Journal of Catalytic Letter*, 97: 163-169.

Tsang, K.Y.2007. Preparation of supported Pt-based mixed nanoparticles and their catalytic properties. Doctor of Philosophy, University of Hong Kong, China.

Tseng, C., Lo,T., Lo,P.and Chu,P.2006.Characterization of Pt-Cu binary catalysts for oxygen reduction for fuel cell applications. *Materials Chemistry and Physics*, 100: 385-390.

Trasatti, S., Grady, W.O., Gerisher, H., and Tobias, C.W. 1981. Advances in Electrochemistry and Electrochemical Engineering, 12: 177 - 261. Wiley, New York.

Tripkovic, A.V., Popovic, K.D., Grgur, B.N., Blizanac, B., Ross, P.N. and Markovic, N.M. 2002. Methanol electrooxidation on supported Pt and PtRu catalysts in acid and alkaline solutions. *Journal of Electrochemistry*, 47(22-23): 3707-3714.

Vishal, M., Dhavale, M., Unni, N., Kagalwala, K., and Pillai, S.2011.Ex-situ Dispersion of Core–Shell Nanoparticles of Cu-Pt on an insitu modified carbon surface and their enhanced electrocatalytic activities. *Journal of Chemical Communication*, 47: 3951–3953.

Wang, Z.B., Yin, G.P., Zhang, J., Sun, Y.C and Shi, P.F.2006. Co-catalytic effect of Ni in the methanol electro-oxidation on Pt-Ru/C catalyst for direct methanol fuel cell. Electrochemistry. *Journal of Electrocatalytic*, 51(26): 5691-5697.

Wang, C., Li,W., Lu,X., Xie, S., Xiao, F., Liu, P. and Tong,Y. 2012.Facile synthesis of porous 3D Co@Ni@Cu nano-network structure and their activity towards hydrogen evolution reaction. *International Journal of Hydrogen Energy*, 37: 18688–18693.

Xiang, X., Li,W., Zhou, Z., Fu ,Z., Lei, J. and Lin ,Y., 2010.Dispersed platinum supported by hydrogen molybdenum bronze-modified carbon as electro catalyst for methanol oxidation. *Journal of Solid State Electrochemistry*, 14: 903-908.

Yang, X., Yan, L., Jiang, X., Wang, X. 2013. Synthesis and photo catalysis of Al doped CdS templated by non-surfactant hypocrellins. *Journal of Environmental Sciences,* 18: 57-578.

Yoo, E., Okada, T., Kizuka, T., Nakamura, J.2008, Effect of carbon substrate material as a Pt-Ru catalyst support on the performance of direct methanol fuel cells. *Journal of Power Sources,* 180: 221-226.

Yueming, L., Longhua, T. and Jinghong, L. 2009. Preparation and electrochemical performanc e for methanol oxidation of pt/graphene nanocomposite. *Electrochemistry Communications*, 11(4): 846– 849.

Zhang, X. and Chan, K. Y. 2002. Microemulsion synthesis and electrocatalytic properties of platinum-cobalt nanoparticles. *Journal of Material Chemistry,* 12: 1203-1206.

Zhang, X. and Chan, K. 2003.Water-in-Oil Micro emulsion Synthesis of Platinum−Ruthenium Nanoparticles, Their Characterization and Electrocatalytic Properties. *Journal of Chemical Material,* 15(2): 451-459.

Zhao, S.,Yang, W., Chen,R.,Wu,X.2010. Towards operating direct methanol fuel cells with highly concentrated fuel. *Journal of Power Sources*, 195: 3451- 3462.

Zhong ,Y.,Wu,W.,Wang,D.,Wang, J.,Shan,L.,Qing,Y. and Zhang.M.2010.Nanogolden wrappe d graphene nanocomposites as trace labels for sensitivity enhancement of electrochemical immunosensors in clinical immunoassays: Carcinoembryonic antigen as a model. Bioelectronics, 25(10): 2379–2383.

Zhou, R., Zheng ,Y., Hulicova, D. and Qia,S.2013.Enhanced Electrochemical Catalytic Activit y by Copper Oxide Grown on Nitrogen-Doped Reduced Graphene Oxide. *Journal of Material Chemistry*, 42: 13179 – 13184.

7. APPENDIX

Appendix Tables

Table 1. The potential difference and peak current of bare Pt/modified electrode in the presence of 1 mM $K_3[Fe(CN)_6]$ in 0.1 M KCl at 50 mV/s

Measurements	Bare Pt	Cu-RGO	Ni-RGO	Ni-Cu/RGO
E_{pa} (mV)	295	297	300	302
E_{pc} (mV)	226	231	236	241
ΔE	69	66	64	61
i_{pa} (mA)	0.864	6.77	8.5	9.8
i_{pc} (mA)	1.18	9.04	10.3	11.5
$i_{pc/}\ i_{pa}$	1.40	1.33	1.21	1.17

Table 2. The effect of scan rate on peak current using Ni-Cu/RGO nanocomposite in the presence of 1mM K_3 Fe $(CN)_6$ in 0.1MKCl

Scan Rate (mV/s)	E_{pa}(mV)	i_{pa}(mA)	E_{pc}(mV)	i_{pc}(mA)	ΔE	$i_{pc/}\ i_{pa}$
10	262	84.2	197	97.7	65	1.16
20	260	132	195	154	65	1.17
50	259	157	196	182.12	63	1.16
75	260	197	198	222.21	62	1.13
100	261	235	200	267	61	1.14

APPENDIX FIGURES

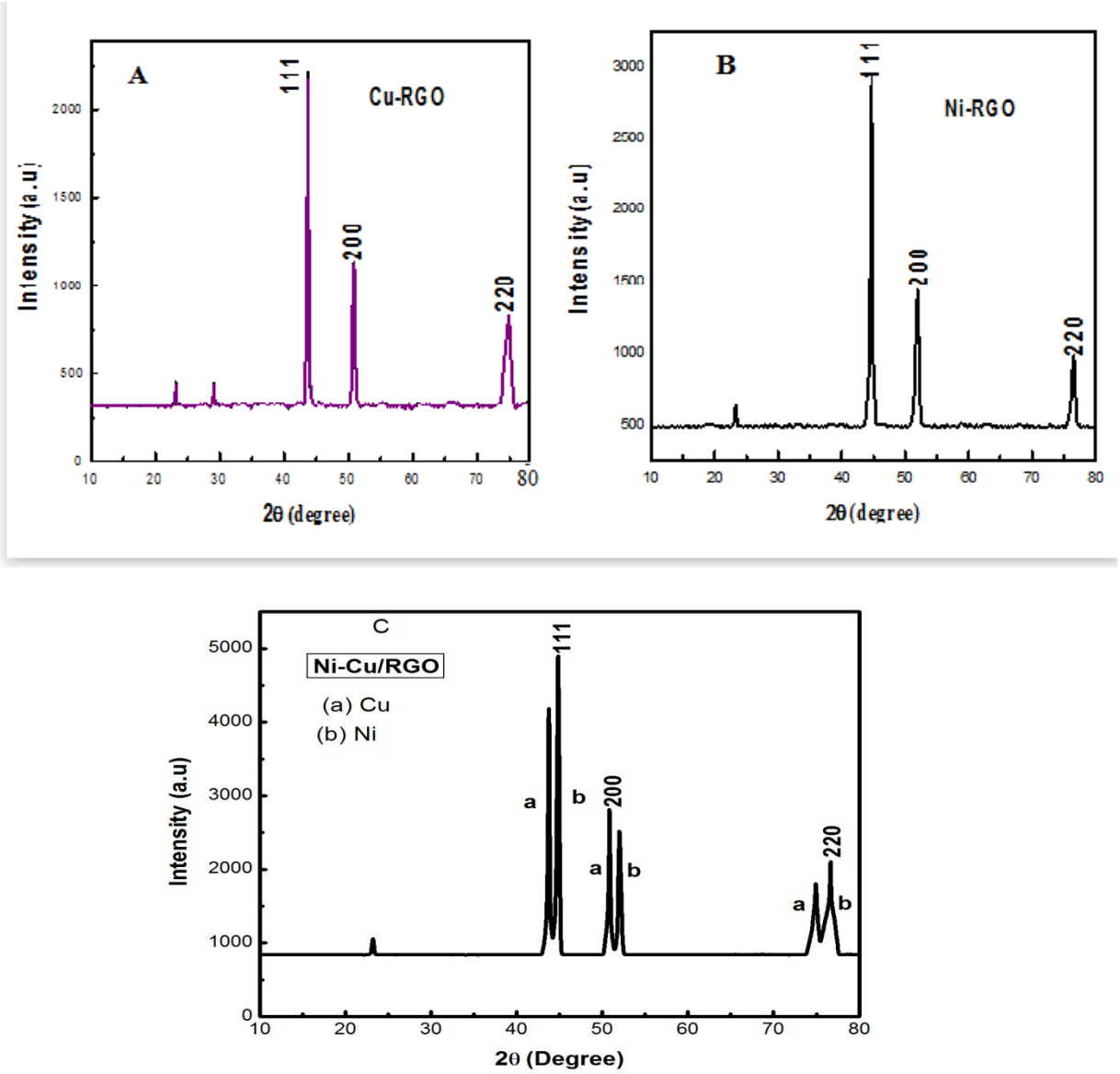

Figure 1. XRD Pattern of result

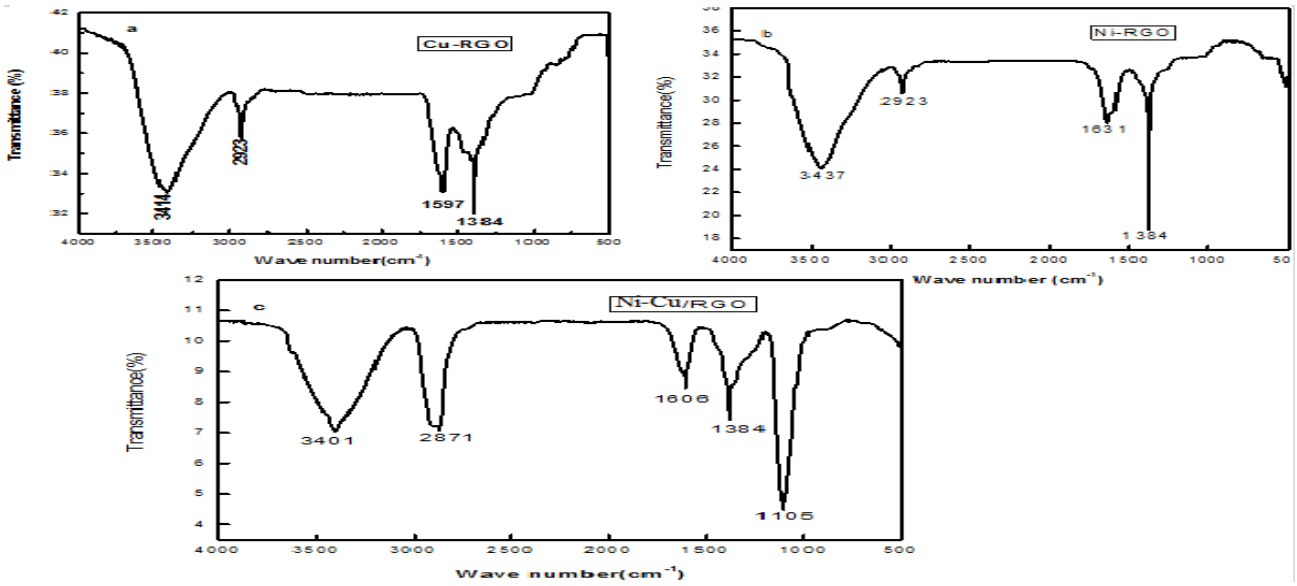

Figure 2. FTIR spectra result

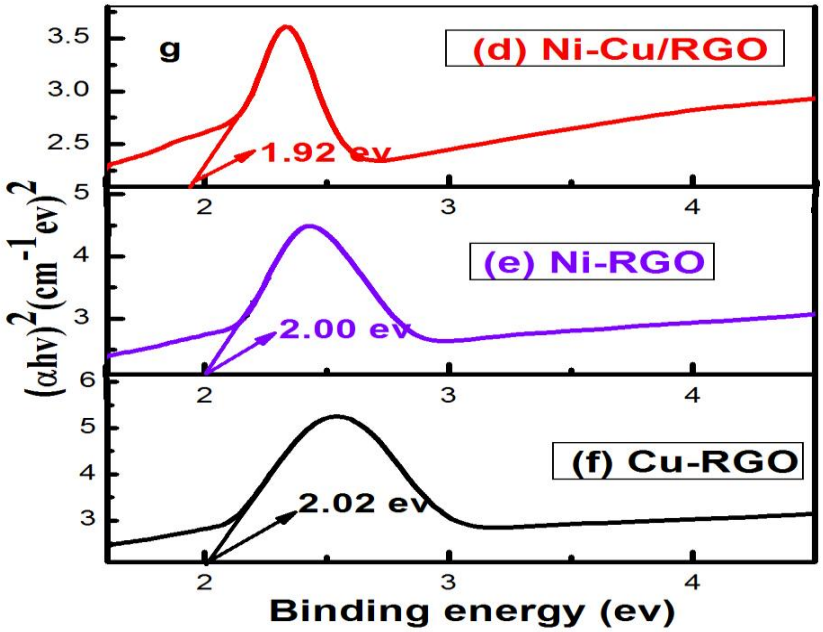

Figure 3. Uv-vis graph for band gap energy determination.